Solar Energy 315 (2026) 114761

Contents lists available at ScienceDirect

Solar Energy

journal homepage: www.elsevier.com/locate/solener

Comparative analysis of adaptive single-objective and multi-objective optimized solar façades for energy efficiency and visual comfort in semi-arid climates

Mohsen Zibaraftar [a,*], Ahmadreza Khalili [b], Shady Attia [c]

[a] Faculty of Art and Architecture, Islamic Azad University South Tehran Branch, Tehran, Iran
[b] School of Engineering, RMIT University, Melbourne, VIC 3000, Australia
[c] Sustainable Building Design Lab, Department UEE, Applied Sciences, University of Liège, Belgium

ARTICLE INFO

Keywords:
Adaptive solar façade
Building integrated photovoltaic
Multi-objective optimization
Energy simulation
Sustainable architecture
Solar building envelope
Visual comfort

ABSTRACT

This article compares the performance of an adaptive single-objective façade system with that of a multi-objective optimized façade, focusing on energy generation and visual comfort in office buildings in semi-arid climates. A kinetic dual-axis PV module was combined with parametric modeling and environmental simulation tools (Rhino/Grasshopper, Honeybee, Radiance, Daysim). It was tested through multi-objective optimization using a genetic algorithm (Octopus). The system was applied to a south-facing office room in Tehran, Iran, and was analyzed during critical seasonal hours. The multi-objective optimized façade achieves Useful Daylight Illuminance (UDI) between 300 and 3000 lx in more than 75% of the task area during the selected occupied hours. It provides superior hUDI compared to the adaptive single-objective façade. The multi-objective optimized system maintained a Daylight Glare Probability (DGP) below 0.35 for all selected critical hours, ensuring visual comfort. Both adaptive single-objective and multi-objective façades demonstrated the potential to reduce energy use by 33.95% and 33.42%, respectively, when compared to an unshaded window, while also enhancing visual comfort. However, implementing an adaptive solar tracking system alone led to potential glare or underlit conditions at certain times, highlighting the trade-off between energy gain and visual comfort. The results of this study indicate that dynamic PV façades can simultaneously enhance energy performance and occupant comfort when optimized by multi-objective optimization frameworks. This research contributes to the development of responsive building envelopes suited for solar-intensive regions.

1. Introduction

Fossil fuel combustion remains a primary source of GHG emissions and drives climate change; therefore, there is a need to shift to renewable energy sources [1–3]. Among these sources, solar energy has gained prominence during the energy transition because it is widely available and can integrate into urban settings [4–6]. Building integrated photovoltaics (BIPV) serves both energy generation and architectural functions while reducing operational energy demand [7–9].

Despite these advantages, vertical BIPV façades are less efficient due to lower solar incidence than rooftop systems [10–13]. Conventional static BIPV installations ignore varying environmental conditions; they produce unwanted visual effects or poor energy harvests [14–16]. Adaptive solar façades (ASF) offer a solution; these systems employ smart materials or mechanical actuators to respond to changing conditions [17–19].

Recent computational design tools and multi-objective optimization methods, including genetic algorithms, improve ASF performance for energy generation and visual comfort simultaneously [20–22]. Yet, few studies have compared single-objective (energy-driven) and multi-objective (energy and visual comfort) optimization approaches for adaptive PV façades. Additionally, the role of mechanical rotation programming and its impact on solar tracking and interior daylight comfort remains understudied.

This study addresses those gaps through three research questions:

1. How does an Adaptive Multi-objective Optimization Façade (AMOF) compare to an Adaptive Single-objective Optimization Façade (ASOF) in balancing energy generation, useful daylight illuminance

* Corresponding author.
E-mail addresses: mzibaraftar@gmail.com (M. Zibaraftar), ahmadreza.khalili@rmit.edu.au (A. Khalili), shady.attia@uliege.be (S. Attia).

https://doi.org/10.1016/j.solener.2026.114761
Received 18 August 2025; Received in revised form 27 April 2026; Accepted 1 June 2026

Nomenclature

Acronyms

ASF	Adaptive Solar Façade
ASOF	Adaptive Single-objective Optimization Façade
AMOF	Adaptive Multi-objective Optimization Façade
BIPV	Building Integrated Photovoltaic
DA	Daylight Autonomy
DC	Direct Current
DGP	Daylight Glare Probability
GCR	Glare Comfort Range
HOY	Hour Of the Year
UDI	Useful Daylight Illuminance
hUDI	hourly Useful Daylight Illuminance
a-si	Amorphous-silicon
hUDI	Fraction of the task area within acceptable UDI thresholds, %
P	Guth position index, –
x	Vector of design variables defining façade configuration (e.g., panel rotation angles)
$f_1(x)$	Objective function for maximizing UDI
$f_3(x)$	Objective function for maximizing PV gen.
DGP_t	Daylight Glare Probability at time step t
N	Total number of evaluated occupied hours or time steps
x_a, x_b	Two different façade design solutions
η_{PV}	Photovoltaic module efficiency (assumed constant)
$\omega_{s\bullet i}$	Solid angle of the i-th glare source based on the viewing position of the observer, sr
T_s	Specular Transmission fraction, –
Sr	Surface Roughness fraction, –
Rs	Specular Reflectance fraction, –
P i	position index of the i-th glare source, –
μF	microfarad
L_s	Luminance of the source, cd/m2
L_{si}	Luminance of the i-th glare source, cd/m2
ω	Solid angle of the source, sr
t	Time, hour
E_v	Vertical illuminance at eye level, lux
W_f	Weighting factor –
E	Illuminance, lux
L	Luminance, nit (or cd/m2)
Ω	Feasible design space of decision variables
$f_i(x)$	Objective function i evaluated for solution x
$f_2(x)$	Objective function for minimizing DGP
UDI_t	Fraction of floor area achieving acceptable daylight illuminance at time step t
$E_{PV,t}$	Photovoltaic electrical energy generated at time step t
T	Set of selected critical hours of the year
$G_{PV,t}$	Solar irradiance incident on the PV surface at time t
A_{PV}	Active photovoltaic surface area

Table 1
Summarize the key differences between some previous ASF systems.

Study	Optimization type	Objectives / Metrics	Climate	Degrees of freedom	Validation type	Includes DGP in optimization?	Single vs Multi comparison?
Nagy et al. (2016)	Single	PV yield	Temperate	Dual-axis	Prototype + measurement	No	No
Hofer et al. (2016)	Single	PV yield	Temperate	Dual-axis	Prototype	No	No
Jayathissa et al. (2017)	Multi	Thermal comfort + PV yield	Temperate	Dual-axis	Simulation only	No	No
PDE – Jayathissa et al. (2018)	Single	PV yield	Temperate	Dual-axis	Simulation only	No	No
Taveres-Cachat et al. (2019)	Multi	PV yield + cDA	Temperate/ hot	Single-axis	Simulation only	No	No
Present study	Multi/Single (for comparison)	PV yield + UDI + DGP	Semi-arid	Dual-axis	Prototype + measurement	Yes	Yes (direct)

(UDI), and daylight glare probability (DGP) in a semi-arid office building context?
2. What is the impact of integrating kinetic mechanisms and control algorithms on the dynamic performance of PV façades?
3. Can adaptive PV façades provide net energy savings while maintaining occupant visual comfort throughout different seasonal solar conditions?

This research develops and evaluates an adaptive PV façade system for dynamic application using parametric tools (Rhino/Grasshopper and Honeybee) in Tehran, Iran, a city with extensive solar resources and visual comfort challenges. Performance is evaluated for energy production and visual comfort metrics (UDI and DGP) under representative seasonal conditions.

The outcomes are expected to offer practical insights into the design of sustainable building envelopes that can enhance occupant comfort and energy efficiency, informing future developments of responsive BIPV systems. Although to date, studies on BIPV, such as Taveres-Cachat et al. (2019) [23] and H. Duan et al. (2025) [24], have shifted their attention to the optimization of static systems for energy savings and visual effects. This study's novelty lies in the first systematic head-to-head comparison of single-objective (energy-only) and multi-objective (energy + visual comfort) optimization on identical kinetic dual-axis PV hardware, quantifying the "cost of comfort" trade-off in semi-arid climates. It is also the first to combine PV energy efficiency with visual comfort metrics (UDI, DGP) using parametric tools, while directly comparing the Adaptive Single-objective Optimization Façade (ASOF) and Adaptive Multi-objective Optimization Façade (AMOF) approaches. By explicitly incorporating Daylight Glare Probability (DGP $<$ 0.35) within the multi-objective framework, this study successfully achieves glare-free performance while maintaining energy efficiency. This approach addresses a gap identified in previous studies conducted in temperate climates, which tended to prioritize daylight autonomy over DGP.

Tehran provides an appropriate case study, characterized by over 2,800 h of annual sunshine and average daily solar radiation of 4.5–5.2 kWh/m^2 [25–28], thereby promoting the viability of BIPV and dynamic façade experimentation. The city's dense urban environment leads to elevated summer cooling demands, increased energy consumption, and pronounced urban heat island effects, exacerbating carbon emissions

Table 2
Comparison between adaptive opaque PV facades (this study) and representative PV glazing technologies.

Feature	Adaptive Opaque PV Façade (This Study)	Semi-transparent PV Windows [82,85]	Colored / Spectrally Selective PV Glazing [84,88]	Nanofluid-based PV / Advanced Glazing Systems [81,83]
Technology type	Opaque building-integrated PV (BIPV) modules with dynamic orientation	Glazing-integrated PV with partial light transmission	PV glazing with spectral filtering or color tuning	Advanced glazing incorporating radiation-regulating materials (e.g., nanofluids)
Light transmission	None (opaque system)	Partial (typically 10–50%)	Partial with modified spectral composition	Variable, depending on fluid/material properties
Impact on indoor daylight	Indirect (via shading and redirection)	Direct transmission of daylight	Direct transmission with altered color spectrum	Direct transmission with dynamic modulation
Impact on color quality (CCT / spectrum)	No spectral alteration (no transmitted light)	May affect color perception depending on PV type	Alters indoor color rendering and spectral distribution	Can modify spectral characteristics dynamically
Primary control mechanism	Geometric control (panel rotation / tracking)	Material properties (transmittance, transparency)	Material-based spectral filtering	Material-based radiation control (dynamic optical properties)
Adaptability	High (dual-axis dynamic adjustment)	Limited (mostly static or low adaptability)	Typically static	Potentially dynamic (depending on system design)
Energy generation principle	Maximization of incident solar irradiance via orientation control	Direct solar conversion with partial transparency	Spectrally selective energy harvesting	Coupled thermal and radiative energy control
Visual comfort control	Achieved through shading optimization and glare reduction (DGP)	Dependent on transmittance; glare risk may persist	May reduce glare but affects color perception	Can improve glare and thermal comfort simultaneously
Glare mitigation	Active (through adaptive shading control)	Passive and limited	Passive	Potentially adaptive
Thermal performance impact	Reduces cooling loads through dynamic shading	Reduces solar gains but may introduce heat through glazing	Similar to semi-transparent PV	Enhanced thermal regulation via fluid properties
Design variables	Panel angles, rotation strategies, control algorithms	Transparency ratio, cell spacing	Spectral properties, coating materials	Fluid type, concentration, optical properties
Optimization approach	Multi-objective optimization (Pareto-based: UDI, DGP, energy)	Typically parametric or single-objective studies	Mostly material optimization	Experimental / material-based optimization
Main research focus	Control strategy comparison (ASOF vs. AMOF)	Material integration into glazing systems	Spectral and aesthetic performance	Advanced energy and radiation control
Application context	External adaptive façade systems	Windows and curtain walls	Architectural glazing systems	Experimental or advanced façade systems
Key limitation	No daylight transmission through PV modules	Trade-off between transparency and efficiency	Color distortion of indoor environment	Complexity and limited real-world deployment

[29]. These conditions mirror challenges observed in other rapidly urbanizing cities located in hot-arid and semi-arid climate zones (as defined by ASHRAE climate classifications), such as *Phoenix*, Albuquerque, Amman, Zaragoza, Cairo, and Dubai. Consequently, while the sustainability strategies explored in this study are locally contextualized, the findings and adaptive façade solutions are expected to be applicable to urban areas with high solar radiation potential, highlighting the importance of optimizing photovoltaic yield alongside glare mitigation.

1.1. Visual comfort quantity

The optimization of visual comfort in workplace settings is crucial for enhancing health and productivity, necessitating a reliable index based on three key factors: quantity, light distribution, and glare, which collectively serve as essential metrics for light assessment [30]. The Useful Daylight Illuminance (UDI) metric, which evaluates the adequacy of daylight (typically 300–3000 lx) across various conditions, is particularly pertinent in hot-arid climates, effectively capturing both underlit and overlit scenarios to comply with comfort standards established by regulations such as Iran's National Building Regulations [31]. For this article, the Useful Daylight Illuminance (UDI) serves as a metric for evaluating visual comfort, encapsulating both glare and daylight intensity within a unified framework by quantifying the annual proportion of time during which the indoor horizontal daylight illuminance at a designated test point meets specified criteria. UDI is a two-tailed metric with lower and upper thresholds defining $UDI_{underlit}$, UDI_{useful}, and $UDI_{overlit}$ ranges (Eq. (1) [32,33].

$$UDI = \frac{\sum_i (wf_i \bullet t_i)}{\sum_i t_i} \epsilon [0 \bullet 1]$$

Where:

$$\begin{cases} UDI_{Overlit} \quad With \quad wf_i = \begin{cases} 1.if\ E_{Daylight} > E_{Upperlimit} \\ 0.if\ E_{Daylight} \le E_{Upperlimit} \end{cases} \\ UDI_{Usefull} \quad With \quad wf_i = \begin{cases} 1.if\ E_{Lowerlimit} \le E_{Upperlimit} \\ 0.if\ E_{Daylight} < E_{Lowerlimit} or\ [30] \\ \quad E_{Daylight} > E_{Upperlimit} \end{cases} \\ UDI_{Underlit} \quad With \quad wf_i = \begin{cases} 1.if\ E_{Daylight} < E_{Lowerlimit} \\ 0.if\ E_{Daylight} \ge E_{Lowerlimit} \end{cases} \end{cases} \quad (1)$$

hourly UDI (hUDI) is computed as the percentage of grid points in the task area that satisfy UDI_{useful} for each analyzed hour, aggregated across the nine critical HOYs. Many people consider daylight illuminance between 300 and 3000 lx to be either ideal or, at the very least, tolerable [30,35]. The 300 lx used for the optimization goal is also the value considered in this article for daylight improvement. Traditional daylight factor approaches often ignore the contribution of sunlight and the variability of real sky conditions [36]; hUDI enhances this by evaluating spatial coverage, defined as the fraction of the task area (e.g., desk plane at 0.7 m height) meeting UDI thresholds during occupied hours, chosen to emphasize practical occupant experience over point-based metrics.

1.2. Visual comfort quality

Glare, according to Hafiz (2015), is the inability to see in the presence of bright light in the field of vision due to a direct or reflected light source [35]. It is commonly expressed as the ratio of the glare sources' size, position, and luminance in the view field to the average luminance, independent of the glare source [30,34]. Generally, it can be formulated by the following equation:

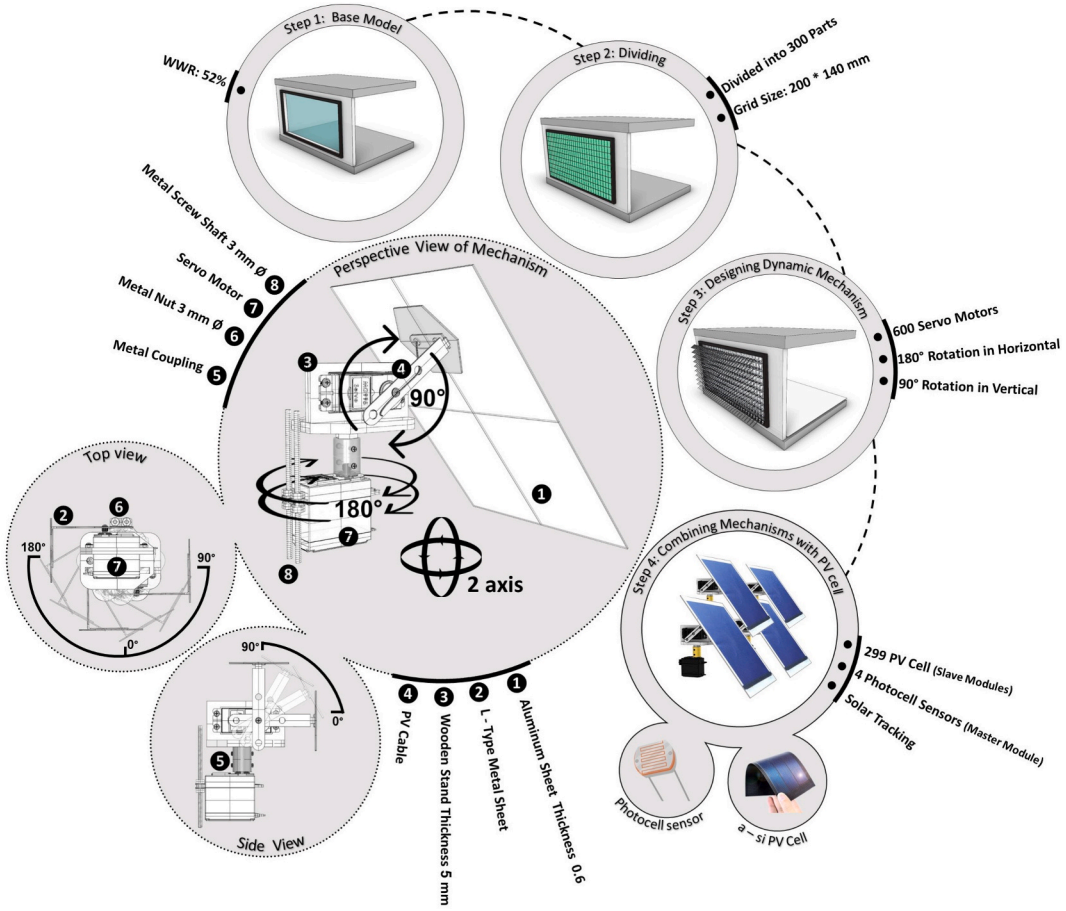

Fig. 1. Detail of mechanism and design process.

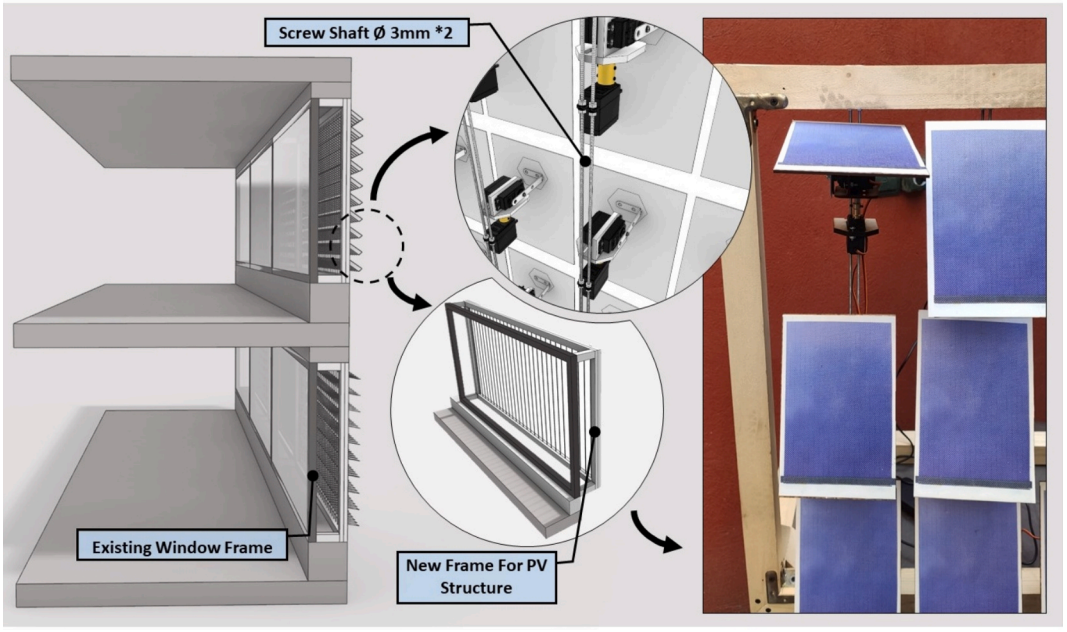

Fig. 2. Left: Details of the window frame and PV module structure. Right: Real view of the experimental prototype.

$$Glare = \sum_{i=1}^{n} \frac{L_{s,i}^{f} \omega_{s,i}}{L_b^g P_i^h} [34] \quad (2)$$

- $L_{s\bullet i}$: Luminance of the i-th glare source (cd/m^2).
- $\omega_{s\bullet i}$: Solid angle subtended by the i-th glare source (sr).
- L_b: luminance of the background (cd/m^2).

Where:

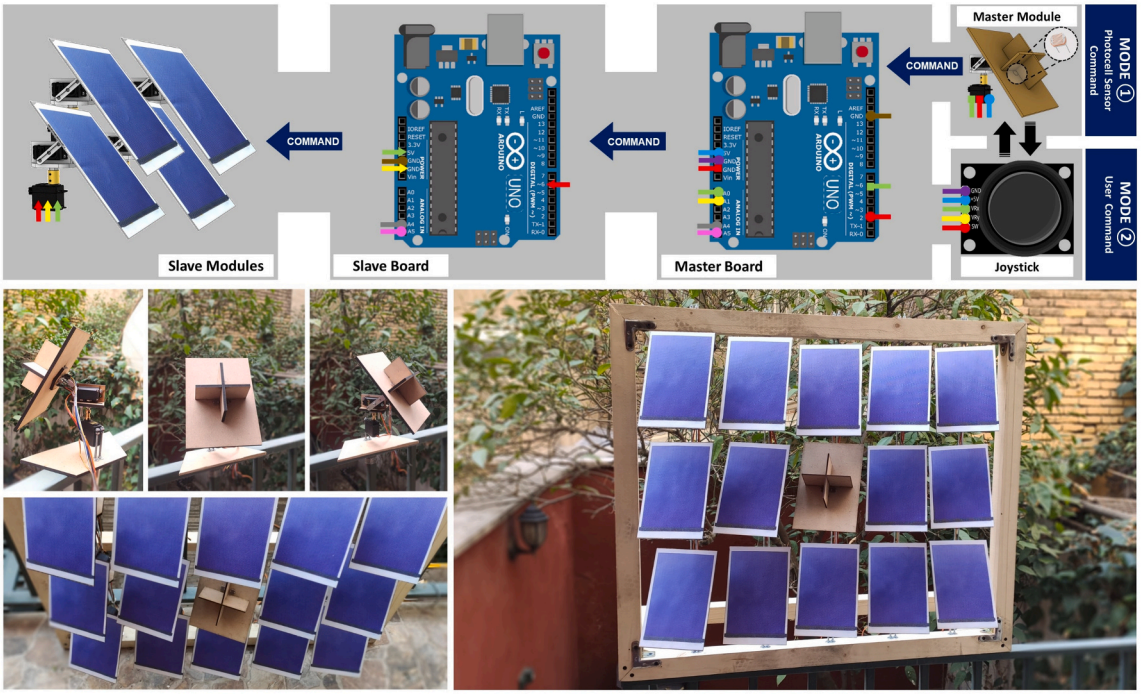

Fig. 3. Top: The I2C communication setup. Bottom: Real view of experimental prototype (master and slave modules).

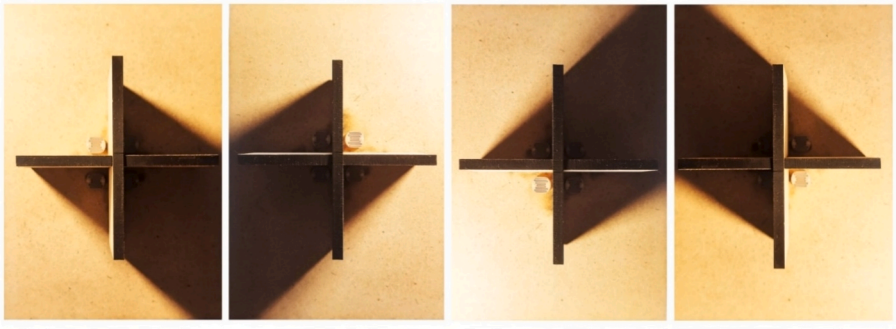

Fig. 4. Front view of the master module with photocell sensors. Display of shadow changes on photocell sensors as the light source moves.

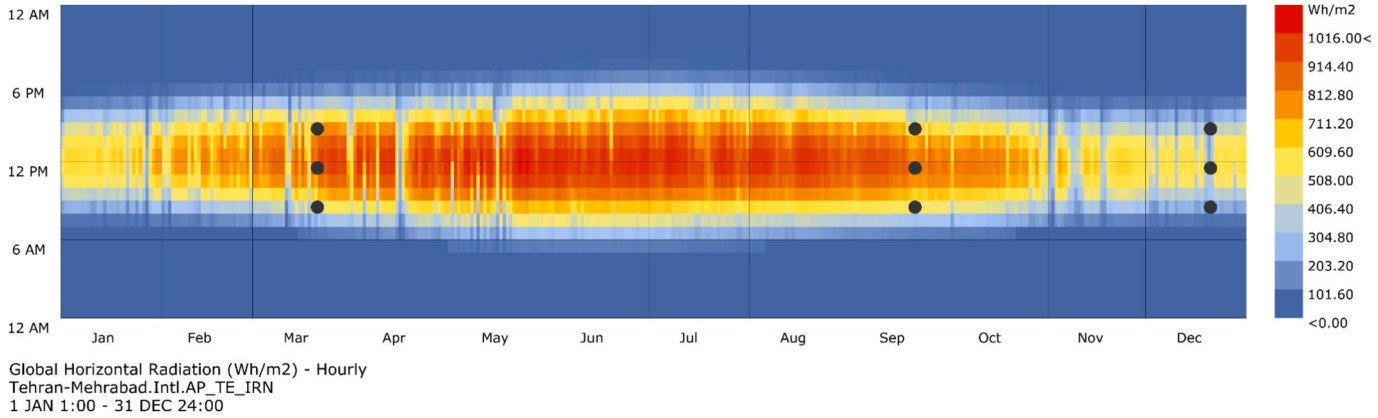

Fig. 5. Global solar radiation and key analysis hours (black dots).

- P_i : Guth position index for the i-th source (accounting for deviation from the line of sight).
- f, g, h : empirical exponential coefficients.

Daylight Glare Probability (DGP) quantifies the proportion of individuals experiencing visual discomfort due to glare (Eq. (3), as articulated by Wienold and Christoffersen (2005) [37]. This metric effectively evaluates glare discomfort by considering luminance

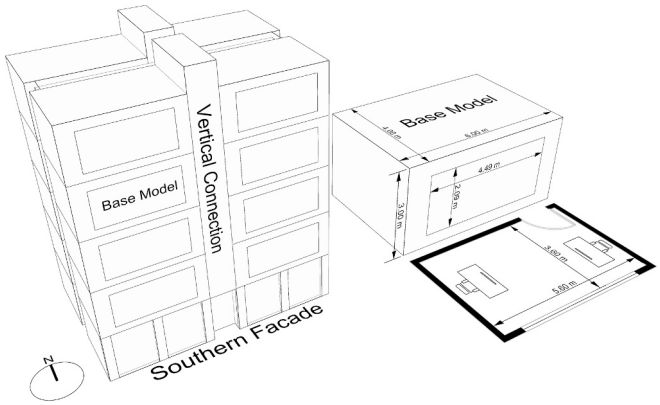

Fig. 6. Left: Case study building geometry. Right: Base model layout.

distributions and occupant positioning, demonstrating superior validation compared to previous indices such as DGI or CGI, particularly in hot-arid environments where high-contrast glare is prevalent [37]. A DGP value below 0.35 is considered imperceptible, while values above 0.45 indicate intolerable glare. The simulation of glare conditions utilized High Dynamic Range (HDR) renderings to assess radiance quantitatively [38]. This process helped determine occupant locations, light levels, and the light sources involved, enabling evaluation of glare levels using the Daylight Glare Probability (DGP) index.

According to Carlucci et al. (2015), the level of discomfort sensation is defined as follows:

More than 0.45 (intolerable), 0.45–0.40 (disturbing), 0.4–0.35 (perceptible), and less than 0.35 (imperceptible) [30,34].

$$DGP = 5 \bullet 87 \times 10^{-5} E_v + 9.18 \times 10^{-5} \log_{10} 2 \left[1 + \sum_{i=1}^{n} \left(\frac{L_{s,i}^2 \bullet \omega_{s,i}}{E_v^{1 \bullet 87} \bullet P_i^2} \right) \right] + 0 \bullet 16 [34] \quad (3)$$

Where:

- E_v : Vertical illuminance at eye level (lux).
- $L_{s \bullet i}$: Luminance of the i-th glare source (cd/m^2).
- $\omega_{s \bullet i}$: Solid angle subtended by the i-th glare source (sr).
- P_i : Guth position index for the i-th source (accounting for deviation from the line of sight).

1.3. Non-Visual effects of Lighting: Illuminance, CCT, and occupant Well-Being

The non-visual effects of lighting, particularly illuminance and Correlated Color Temperature (CCT), are critical in influencing occupant mood, alertness, and circadian health in office settings [39,40]. Enhanced alertness and cognitive performance are associated with higher CCT levels (e.g., 5000–6500 K), while lower CCT ranges (2700–4000 K) promote relaxation but may hinder productivity [41–44]. Although CCT is vital for visual comfort and circadian response [45,46], it was excluded as an optimization criterion in this study due to the opaque nature of the utilized amorphous-silicon PV modules, which do not permit daylight transmission.

By integrating UDI, DGP, and PV performance into a validated, climate-specific ASF model, this work provides a robust methodology for the design and control of high-performance adaptive façades.

Some of the significant processes, approaches, opportunities, and gaps relevant to this article are briefly highlighted in the literature that follows.

1.4. Literature review

1.4.1. Adaptive solar Façades (ASF): Concepts and mechanisms

Adaptive solar façades (ASF) integrate solar photovoltaic (PV) modules within dynamic envelope systems to maximize energy performance and visual comfort. Nagy et al. (2016) introduced a pioneering ASF system that achieved a 36% increase in energy output [47]. Integration of adaptive façades with thin-film PV technologies also enhances building-integrated photovoltaic performance. Actuator energy consumption, however, has received insufficient exploration and poses scalability issues. Hofer et al. (2016) demonstrated more than 50% enhancement in PV output through the integration of thin-film modules with adaptive shading. The authors created a method that relies on parametric 3D and electrical simulations to model dynamic shading and energy yield, although implementation obstacles continue in dense urban areas [48]. Jayathissa et al. (2017) combined dynamic BIPV shading with thermal and daylight simulation, and realized 20–80% net energy savings. They presented an adaptive control strategy for the PV panel orientation based on the interaction between dynamic photovoltaic shading systems and building energy demands, but the visual comfort was not optimized [49]. A subsequent study by Jayathissa et al. (2018) developed a parametric design environment (PDE) that generates four key outputs: manufacturing plans, visual renders, energetic performance, and structural performance to balance energy and daylight outcomes [50]. However, the limitations include high computational loads and potential software errors. Michael et al. (2018) proposed a dynamic environmental skin façade system for existing structures, aiming to improve indoor visual comfort and energy efficiency [51]. The efficacy of this adaptive shading mechanism is evaluated via software simulations, given the lack of previous research, with particular emphasis on retrofitting conventional office environments in historic European buildings. Bratislav et al. (2019) applied full-scale prototypes to examine actuator precision, which supports ASF feasibility even with cost and durability concerns [52]. Sureshkumar et al. (2024) employed parametric modeling to adjust panel angles dynamically and optimize solar radiation control. This approach reduces glare while preserving adequate daylighting. A Melbourne case study indicated that kinetic BIPV façades reduce energy consumption and demand through PV generation, yet reliance on simulation and the lack of experimental validation weakened the results [53].

1.4.2. Multi-objective optimization frameworks for building envelopes

The evolution of building envelope optimization has increasingly adopted multi-objective approaches to simultaneously address energy performance, visual comfort, and economic considerations. Delgarm et al. (2016) demonstrated the effectiveness of simulation-based multi-objective optimization using MOPSO and EnergyPlus, achieving significant reductions in annual energy demand across different Iranian climates, particularly in cooling loads [54]. Similarly, Naderi et al. (2020) and Acar et al. (2021) showed that optimized envelope parameters and control strategies can substantially reduce energy consumption while improving occupant comfort and lifecycle cost performance [55 56].

Several studies have focused on optimizing shading systems and façade geometries. Taveres-Cachat et al. (2019) and Kirimtat et al. (2019) applied multi-objective optimization to parametrically designed shading devices, improving energy and daylight performance, although often limited to fixed systems or simplified climatic assumptions [23 57]. Later studies, including Nazari et al. (2023) and Liu et al. (2024), further explored the influence of shading geometry and control strategies, highlighting the importance of parameters such as slat configuration and orientation in reducing energy consumption and improving daylight performance [58 59]. However, many of these approaches remain constrained by static configurations or limited adaptability.

In parallel, optimization frameworks integrating advanced computational methods have been developed. Kim and Clayton (2020) introduced a Parametric Behavior Map (PBM) approach for climate-adaptive

Table 3
Simulation parameters and performance metrics.

Model Parameters	Site Location:		Tehran, Iran (35.7219° N, 51.3347° E)		
	Weather Data Source:		Energy Plus Weather File (EPW)[91]		
	Function and Space Area:		Single office room, 24 m^2		
	Design Objectives:		a)Maximizing Hourly Useful Daylight Illuminance (hUDI), b) Minimizing Daylight Glare Probability (DGP), c)Maximizing incident radiation on PV modules		
	Visual Comfort Design Requirements:		UDI Threshold: 300 to 3000 Lux Acceptable DGP: Lower than 0.35 Acceptable GCR: Imperceptible glare		
Performance Criteria	**Parameters**		**Name**	**Unit (Symbol)**	**Range**
	Daylight Parameters:		UDI (Underlit)	Lux (lx)	[0–300]
			Useful Daylight Illuminance	Lux (lx)	[300–3000]
			UDI (Overlit)	Lux (lx)	[>3000]
	Glare Parameters:		Daylight Glare Probability	Decimal no.	[0.0—1.0]
			Glare Comfort Range a) 0 = imperceptible;1 = perceptible; 2 = disturbing; 3 = intolerable	Integer	[1–3][a]
	Model Variable Parameters:		Module Vertical Angle	Degree (°)	[0° to 90°]
			Module Horizontal Angle	Degree (°)	[-90° to 90°]
			Indoor View Angles a) 0 = Towards outdoor;1 = Front view; 2 = 45 Degrees towards outdoor	Integer	[1,2][a]
	Model Fixed Parameters:	Dimension	Glazing Ratio	Percentage (%)	52
			Task Area Height	Centimeter (cm)	70
			Room Width	Centimeter (cm)	400
			Room Length	Centimeter (cm)	600
			Room Height	Centimeter (cm)	300
		Material	Glass Transmittance	Percentage (%)	70
			Int. Wall Reflectance	Percentage (%)	50
			Int. Ceiling Reflectance	Percentage (%)	80
			Int. Floor Reflectance	Percentage (%)	20
		PV Cell Specification	Brand: JIANG SOLAR [92]		
			Material: Amorphous Silicon	(a-Si)	
			Specular Transmission	(T_s)	0
			Dimension	Centimeter (cm)	20 × 14
			Thickness	Millimeter (mm)	1
			Weight	Gram (g)	47
			No − Load Voltage	Volt (V)	1.9
			Load Voltage	Volt (V)	1.5
			Power	Watt (W)	1.5
			Short Circuit Current	Ampere (A)	1.2
			Efficiency	Percentage (%)	10
			Cost of Each Module	USD ($)	17
	Time Parameters:		Month	Integer	[1,2][a]
			Day	Integer	21
			Hour a) 0 = March;1=September; 2 = December	Integer	[9,12,15]

envelopes, though limited to a short simulation period [60]. Xu et al. (2021) and Ghaderian and Veysi (2021) employed hybrid methods combining artificial neural networks, surrogate models, and evolutionary algorithms to optimize energy and comfort performance, demonstrating improved computational efficiency and reliability [61 62]. Similarly, BIM- and machine learning-based frameworks have been applied to optimize energy use and thermal comfort in educational buildings [63].

Other studies have investigated adaptive façade systems and control strategies. Pilechiha et al. (2020) proposed a multi-objective framework for balancing daylight, energy efficiency, and quality of view in office environments [64], while Lee et al. (2021) demonstrated the effectiveness of adaptive solar façade (ASF) control strategies in improving both energy and visual comfort [65]. Bakmohammadi and Noorzai (2020) further enhanced optimization performance through a two-phase approach focusing on lighting energy reduction and detailed visual comfort analysis [66]. Additionally, Rizi and Eltaweel (2021) explored textile-based adaptive shading systems to improve thermal and visual comfort, although without experimental validation [67].

Recent research has expanded toward data-driven and high-dimensional optimization frameworks. Tharushi Imalka et al. (2024) applied data-driven optimization to balance energy, cost, and comfort, while Qi et al. (2025) introduced a novel kirigami-inspired photovoltaic shading façade, highlighting trade-offs between visual comfort and

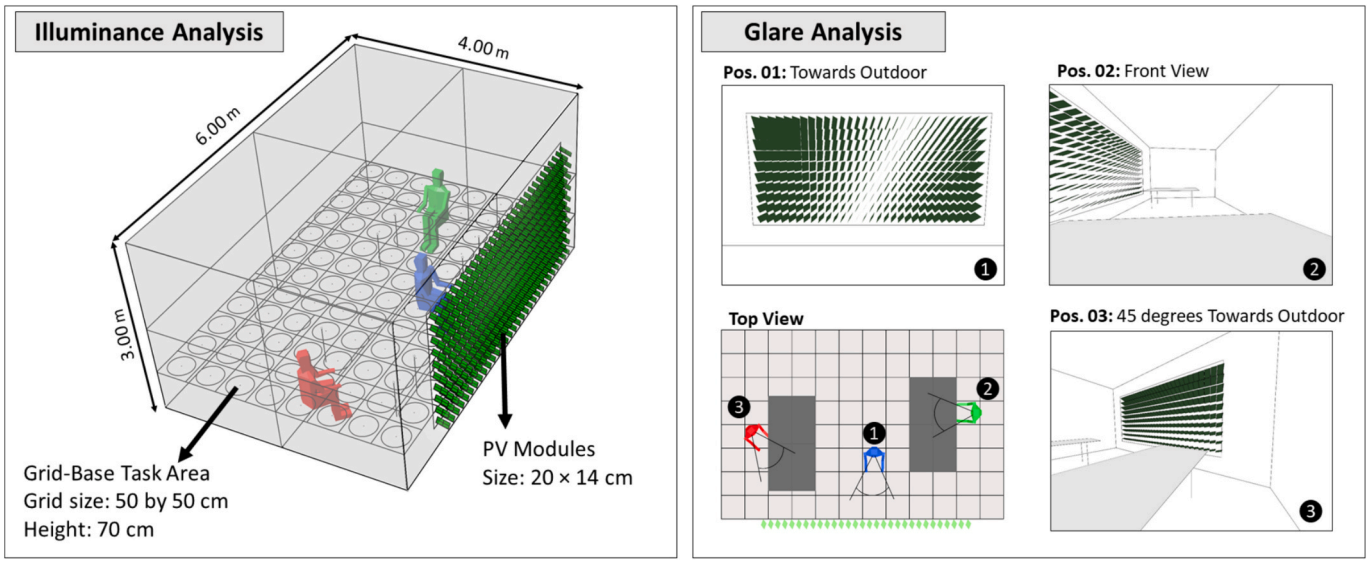

Fig. 7. Left: Illuminance analysis setup. Right: Glare analysis with three different views.

daylight availability [68 69]. Similarly, Yang et al. (2025), Chen et al. (2025), Zhang et al. (2025), and Duan et al. (2025) developed advanced multi-objective optimization frameworks integrating PV systems, façade geometry, and environmental variables, although often limited by simplified assumptions, lack of economic considerations, or reliance on fixed shading configurations [70 71 72 24].

Finally, similar studies in Australia, the USA, Chile, India, Algeria, Singapore, and China explored envelope configurations, motion types [73], glazed photovoltaic thermal systems [74,75], blind control via NSGA-II, BIM [76], machine learning, and hybrid optimization (e.g., MUZO-MPOA-PSO-SVM-NSGA-II) [77–80].

1.5. Research gaps and contributions of this study

As indicated in Table 1, in spite of growing interest in ASF systems and multi-objective optimization (MOO), significant gaps persist. Primarily, comparative analyses of single-objective (e.g., energy-only) and multi-objective (e.g., energy + comfort) optimization frameworks are rare. Second, the majority of the research does not describe the incorporation of actuator programming and control logic in dynamic systems. Lastly, few works address the collective effect of Useful Daylight Illuminance (UDI), Daylight Glare Probability (DGP), and incident solar radiation under a single MOO framework.

This study makes a novel contribution by systematically comparing adaptive single-objective and multi-objective façade control in a dual-axis PV-integrated ASF prototype. In contrast with prior studies (e.g., Nagy et al., Jayathissa et al.), the current research demonstrates the model's performance in the real world for the semi-arid Tehran case using empirical measurements.

In summary, the literature review demonstrates remarkable progress in adaptive solar façades and multi-objective optimization frameworks but also underscores unresolved issues in the incorporation of real-time control, empirical verification, and balanced comfort-performance trade-offs. Most previous studies rely heavily on simulation, often omitting the actuator control logic, climate-specific verification, or a balanced consideration of energy, daylight, and glare. This study addresses these gaps by presenting a fully operational, dual-axis ASF prototype with servo-driven actuation, verified using a genetic algorithm-based optimization method. By integrating metrics such as UDI, DGP, and PV generation in a real-world setting, the research establishes a new benchmark for data-driven design and control of high-performance adaptive façades. It is important to note that this study does not introduce a new photovoltaic shading or glazing technology. The dual-axis ASF system already exists as an opaque BIPV module, and this work contributes by comparing two control strategies, ASOF and AMOF, in terms of daylight performance, glare, and energy generation.

1.6. Comparing Alternative BIPV technologies

Recent innovations in radiation-regulating BIPV materials, such as ATO nanofluids and colored semi-transparent windows, offer new energy harvesting and daylighting strategies [81]. These technologies selectively manage the solar spectrum to optimize energy generation, thermal gains, and occupant comfort [82]. ATO nanofluid-enhanced PV windows facilitate heat management by absorbing near-infrared radiation while transmitting visible light, potentially reducing cooling loads [83]. However, in semi-arid climates like Tehran, direct-beam transmission can raise DGP above 0.35, compromising glare-free performance compared to opaque adaptive systems that completely block direct radiation when necessary. Colored and semi-transparent BIPV windows enhance aesthetics but may alter spectral properties, impacting CCT and CRI, thus affecting occupant well-being [84,85]. The opaque kinetic PV façade is different because it acts as an external shading device, effectively mitigating glare, avoiding spectral changes, and ensuring neutral light quality alongside energy savings without advanced materials [86]. In contrast, while nanofluid-enhanced PV windows can lower energy consumption via heat decoupling [87], they may still permit excessive direct radiation, increasing DGP in clear-sky scenarios. Therefore, Table 2 provides a summary of the information mentioned above.

This comparison shows that the opaque kinetic PV façade system improves dynamic control and optimization strategies on existing hardware, providing superior glare-free performance and measurable energy-comfort trade-offs in solar-intensive regions, areas where new materials alone may not be enough without adaptive mechanisms.

2. Methodology

This section presents the methodological framework for evaluating the adaptive photovoltaic (PV) façade system in terms of visual comfort and energy performance. The simulation workflow in the ASOF mode is to increase solar radiation and, consequently, energy production through solar tracking by PV modules, while in the AMOF mode the workflow consists of increasing visual comfort and energy production simultaneously through multi-objective optimization. The workflow integrates parametric modeling, environmental simulation, and multi-

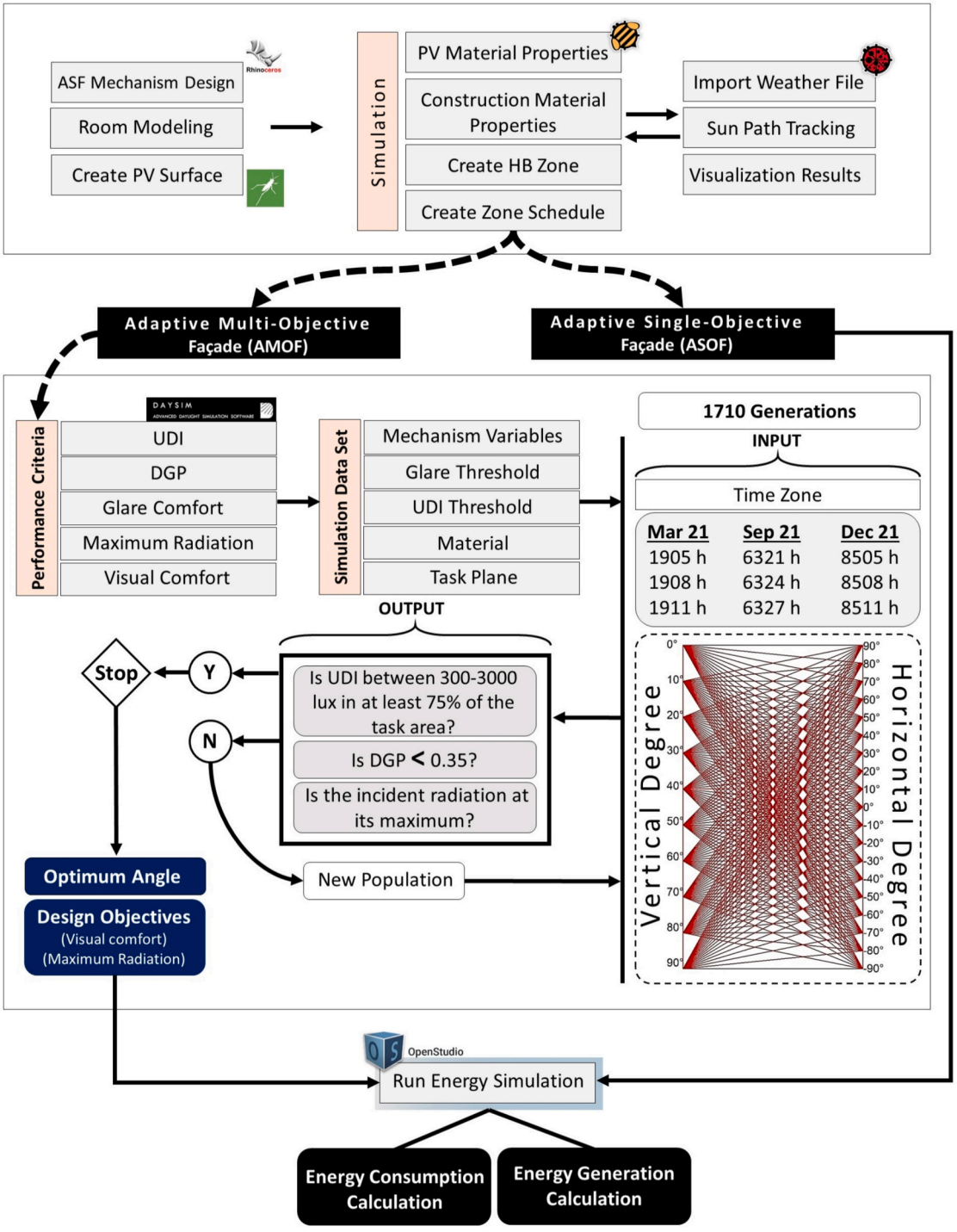

Fig. 8. Control strategy and modeling process.

objective optimization. Rhino/Grasshopper were utilized for parametric modeling, enabling adaptive design integration and environmental simulations via Honeybee plugins. The simulation workflow included: (1) daylight illuminance calculations for Useful Daylight Illuminance (UDI), (2) glare assessment through Daylight Glare Probability (DGP), (3) electrical energy generation analysis based on incident irradiance on PV modules, and (4) building energy use simulations for heating, cooling, and electric lighting. Multi-variable inputs, such as rotation angles, seasonal hours, and façade configurations, were evaluated to identify control strategies that balance daylight performance, glare reduction, and energy generation. This integrated approach provides a consistent basis for comparing the ASOF and AMOF modes.

2.1. Concept and mechanism design

The study focuses on evaluating an adaptive photovoltaic (PV) façade system by comparing two control strategies for dynamic solar modules, rather than introducing a new hardware concept. As illustrated in Fig. 1, the system employs a dual-axis rotation mechanism powered by two servo motors mounted perpendicularly, enabling each PV module to adjust its orientation in real time. This configuration allows the façade to enhance incident solar radiation and optimize both energy

Table 4
Input parameters for energy simulation assumptions.

Parameters	Value
Interior Wall Thickness	0.2 *m*
Floor to Floor Distance	3.00 *m*
HVAC System	Packaged rooftop (VAV) variable air volume
Cooling Setpoint	24 °C
Cooling Setback	27 °C
Heating Setpoint	20 °C
Heating Setback	15 °C
Lighting Level	500 Lux
Lighting Power Density Per Area	10 W/m^2
Equipment Load Per Area	8 W/m^2
Peak Occupant Load	10 m^2/ppl
Infiltration rate per area*	0.0006 m^3/s-m^2
Ventilation Per Area	0.00045 m^3/s-m^2

*According to ASHRAE recommendations for leaking buildings and poor construction details in the study setting.

generation and visual comfort under varying seasonal and hourly conditions. An experimental prototype of the mechanism was developed to validate the irradiance performance of the PV modules under controlled movements. The prototype served exclusively for measurement-based validation and was not used in the optimization process. All optimization, daylight simulations, and visual comfort evaluations were conducted within the parametric modeling and simulation workflow described in Sections 2.2–2.4.

2.1.1. PV module rotation structure

Servo motors facilitate rotations of up to 180 degrees horizontally and 90 degrees vertically. Metal shafts hold the 20 × 14 cm PV modules mounted on the window frame. Each module includes servo motors, PV layers, and structural units (Fig. 2).

2.1.2. Module rotation programming for ASOF mode

Arduino IDE 1.8.13 (C++) was used for programming. Modules communicate via the I2C protocol, with one master and multiple slave modules (Fig. 3) [89].

The master module operates in two modes:

- Adaptive Mode: As shown in Fig. 4, four photocell sensors detect light intensity (0–1023). A mathematical algorithm determines the brightest direction and adjusts servo angles accordingly (Appendix A).
- User Mode: Manual joystick control adjusted angles. Slave modules synchronized with the master module (Fig. 3).

2.2. Case study setup

The case study examined an office room in Tehran (35.7219° N, 51.3347° E) that demonstrates significant potential for solar cell use. Fig. 5 illustrates the annual variation in global solar radiation, with selected points corresponding to March 21, September 21, and December 21, based on LEED v4 EQ Daylight – Option 2 (Illuminance simulation), which guided the selection of the seasonal analysis dates [90]. To make the optimization more robust for the specific challenges of a south-facing façade in a semi-arid climate, where the lowest solar altitudes in winter create the highest direct-beam penetration and glare risk, the following items were extended to the standard LEED v4:

- Adding the 12:00 noon on both equinoxes (21 March & 21 September) represents intermediate or balanced solar conditions, characterized by moderate solar altitudes and symmetrical day–night durations.
- Adding the full three times (9:00, 12:00, 15:00) on the winter solstice (21 December). The solar altitude is at its annual minimum, leading to reduced solar penetration depth and the most challenging conditions for achieving adequate daylight availability.

These representative dates are widely adopted in studies evaluating daylight performance metrics such as Useful Daylight Illuminance (UDI) and Daylight Glare Probability (DGP), as well as in simulation-based investigations using Radiance, Daysim, and adaptive façade systems, to capture extreme and typical daylighting scenarios throughout the year.

As shown in Fig. 6, the module was tested on a south-facing façade (WWR 52%) with a single-zone working space measuring 6 m × 4 m × 3 m. The room is located on the middle floor of a multi-story building, with an approximate area of 650 m^2. With the exception of the façade facing south and west, it is surrounded by other office spaces. The façade and the remainder of the wall are therefore regarded as adiabatic.

Table 3 summarizes all fixed and variable parameters used in the optimization and simulation process, including geometry, material properties, PV specifications, and analysis hours.

UDI and glare metrics evaluated daylight and visual comfort. Grid-based daylight simulation, referencing UDI thresholds, such as hourly Useful Daylight Illuminance (hUDI) and glare comfort range, optimized

Table 5
Sky condition and rendering options. The portion of the sky dome, measured in tenths, that is covered by clouds or other obscuring phenomena at the specified hour. (i.e., 1 is 1/10 covered. 10 is total coverage. Energy Plus Weather File (.epw) [91].

Hourly sky cover of Tehran

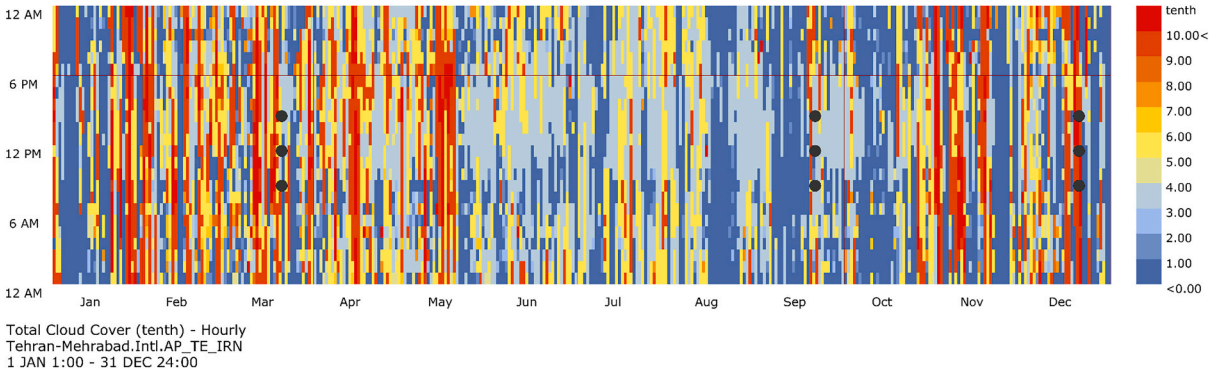

Accurate Setting Rendering Options
−ab: ambient bounces = 2 −aa: ambient accuracy = 0.15 −ar: ambient resolution = 128 −ad: ambient divisions = 512 −as: ambient super-samples = 256

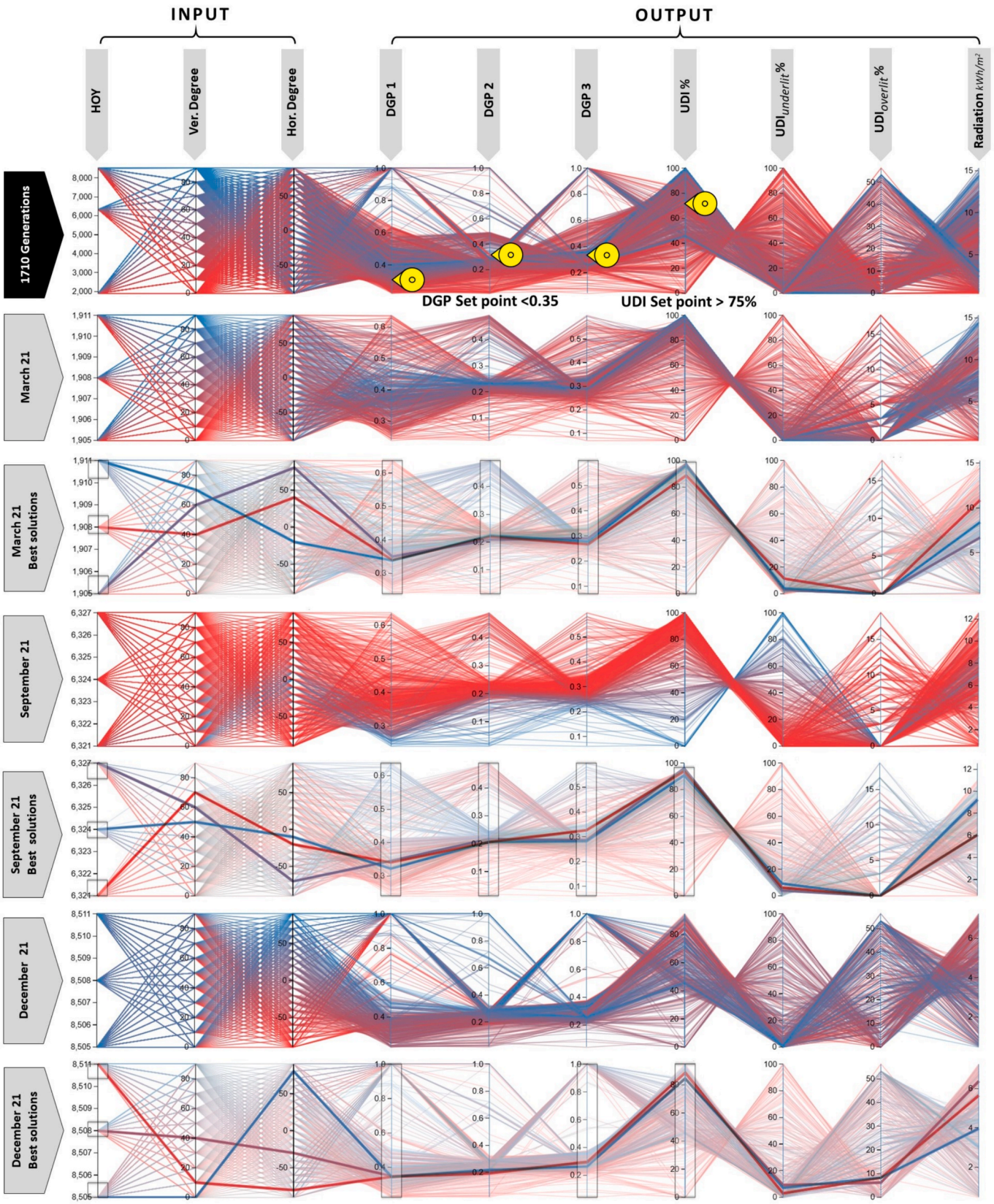

Fig. 9. The visualization of a full dataset of solutions with the aim of facilitating exploration.The optimum angles for PV modules in nine HOYs in AMOF mode.

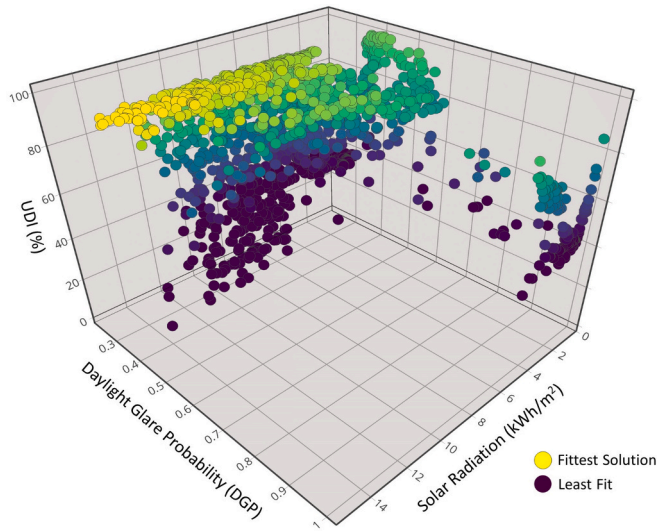

Fig. 10. The full dataset of potential solutions. The Pareto-optimal solutions, highlighted in yellow, represent the best trade-offs among the objectives. (For interpretation of the references to colour in this figure legend, the reader is referred to the web version of this article.)

façade layers for a 70 cm-high task area (Fig. 7).

2.3. Multi-objective optimization setup for AMOF mode

A Genetic Algorithm (GA) via the Octopus plugin optimized three objectives:

1. Maximize PV irradiance
2. Maintain UDI between 300–3000 lx in at least 75% of the task area [90]
3. Minimize DGP

Honeybee/Radiance/Daysim integration improved simulation accuracy [93]. The multi-objective optimization procedure performed with Octopus, with a population size of 1710, was carried out over 9 Hours of the Year (HOYs) and 9 vertical angles and 18 horizontal angles, resulting in 100 generations to construct a complete Pareto-front. A mutation rate of 0.9, a mutation probability of 0.2, and a crossover rate of 0.8 were applied to maintain genetic diversity while stabilizing the optimization trajectory. In the first phase, Octopus GA selected Pareto-optimal solutions, and the full dataset were exported to Microsoft Excel for analysis. The second phase identified the best angles between optimal solutions for balancing UDI and DGP while also maximizing solar radiation via "Design Explorer". The final phase assessed energy generation and use, comparing the baseline window to the ASOF and AMOF modes. The genetic algorithm applies a Pareto-based multi-objective optimization approach, treating UDI maximization, DGP minimization, and PV irradiance maximization equally. Solutions are evaluated according to Pareto dominance, enabling the identification of balanced configurations without prioritizing one objective over another. This approach is particularly suitable for adaptive façade systems, where energy generation and visual comfort indicators naturally involve trade-off relationships. The optimization process can be formulated as:

$$Minimize/MaximizeF(x) = [f_1(x), f_2(x), \cdots, f_n(x)] \quad (4)$$

Subject to: $x \in \Omega$

Where.

- (x) Represents the vector of design variables defining the façade configuration (e.g., panel rotation angles)
- Ω denotes the feasible design space
- $f_i(x)$ are the objective functions representing energy and visual comfort performance metrics

Based on the scope of this study, the following objective functions were defined:

(1) Maximization of useful daylight availability.

The Useful Daylight Illuminance (UDI) metric was used to evaluate daylight quality. The objective was defined as:

$$f_1(x) = \max\left(\frac{1}{N}\sum_{t=1}^{N} UDI_t(x)\right) \quad (5)$$

Where

HOY	March 21			September 21			December 21		
	1905	1908	1911	6321	6324	6327	8505	8508	8511
Vertical Angle (Degree)	60	40	70	70	50	60	0	40	10
Horizontal Angle (Degree)	80	40	-20	-20	-10	-70	80	-30	-80
Front View of PV Modules									

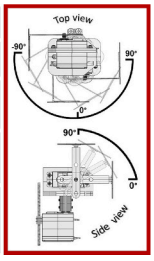

Fig. 11. PV modules' optimal angles in nine HOYs in AMOF mode, as determined by the best solutions.

Table 6
Comparison of UDI results across three modes.

		Unshaded Window			(ASOF)			(AMOF)		
	HOY	UDI (%)	$UDI_{overlit}$ (%)	$UDI_{underlit}$ (%)	UDI (%)	$UDI_{overlit}$ (%)	$UDI_{underlit}$ (%)	UDI (%)	$UDI_{overlit}$ (%)	$UDI_{underlit}$ (%)
March 21	1905	80.21	19.79	0	86.46	0	13.54	96.87	0	3.12
	1908	71.88	28.13	0	96.88	0	3.13	88.54	0	11.45
	1911	77.08	21.88	1.04	90.63	0	9.38	95.83	0	4.16
September 21	6321	80.21	19.79	0	87.5	0	12.5	93.75	0	6.25
	6324	77.08	22.92	0	96.88	0	3.13	90.62	0	9.37
	6327	77.08	21.88	1.04	90.63	0	9.38	95.83	0	4.16
December 21	8505	**48.96**	51.04	0	**62.5**	0	37.5	84.37	8.33	7.29
	8508	**43.75**	56.25	0	**62.5**	6.25	31.25	84.37	8.33	7.29
	8511	**45.83**	53.13	1.04	**33.33**	0	66.67	88.54	8.33	3.12

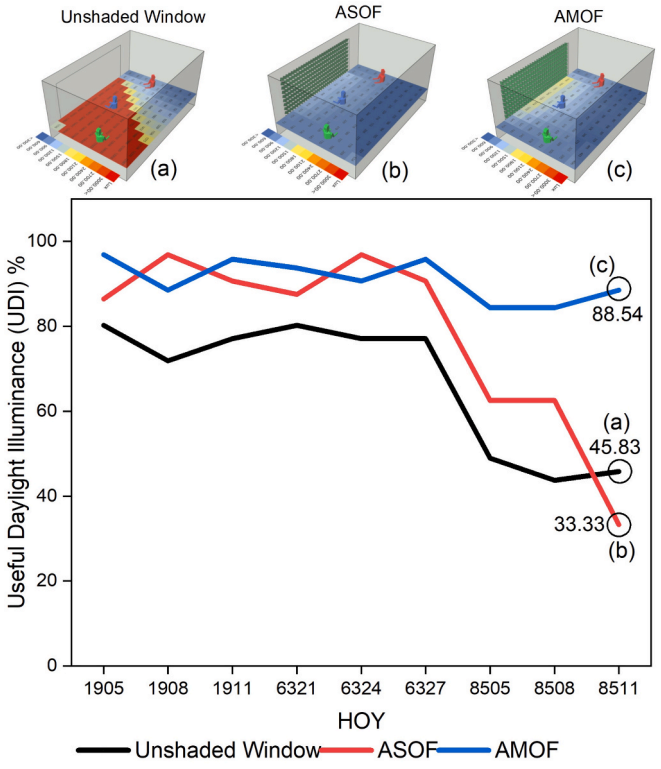

Fig. 12. UDI performance. Demonstrating AMOF's consistent performance in terms of UDI criteria.

- UDI_t represents the fraction of the occupied task area achieving illuminance within the acceptable range (300–3000 lx) at time step t_1
- N is the total number of evaluated occupied hours

(2) Minimization of daylight glare probability.

Visual discomfort due to glare was quantified using Daylight Glare Probability (DGP). The objective was formulated as:

$$f_2(x) = \min\left(\max_{t\in T} DGP_t(x)\right) \tag{6}$$

Where

- DGP_t denotes the glare probability at time t_1
- T represents the set of selected critical hours of the year.

A threshold of DGP < 0.35 was considered indicative of acceptable visual comfort.

(3) Maximization of solar PV irradiance.

The photovoltaic energy output was defined as:

$$f_3(x) = \max\left(\sum_{t=1}^{N} G_{PV,t}(x)\right) \tag{7}$$

Where

- $G_{PV,t}$ is the solar irradiance incident on the PV surface at time t [W/m^2]
- x Is the panel rotation angles

PV electrical energy is then estimated as:

$$E_{PV,t} = \eta_{PV}.A_{PV}.G_{PV,t} \tag{8}$$

Where

- η_{PV} PV module efficiency
- A_{PV} active PV area

Because η_{PV} and A_{PV} are constant, maximizing irradiance is mathematically equivalent to maximizing PV energy generation.

The optimization process generated a Pareto-front representing non-dominated solutions, capturing the trade-offs between energy performance and visual comfort. No explicit weighting factors were assigned to the objective functions. Fig. 8 offers a graphic representation of the continuous feedback loop when investigating the control strategy. Simulations took place at 9:00, 12:00, and 15:00 on three key dates spanning HOYs 1905–8511.

2.4. Energy generation and consumption simulation

The Honeybee plugins were used to model the energy use of the lighting, heating, cooling, and electrical load. The input parameters for energy simulation are summarized in Table 4. The building's HVAC system is regarded as a packaged rooftop VAV (variable air volume) system with reheat. This system uses a hot-water fossil-fuel (natural gas) boiler for heating, chilled water for cooling, and variable-air-volume (VAV) for fan control. Table 3 displays the building material characteristics, encompassing the floor, walls, and ceiling. These materials are considered common construction materials in Tehran's official buildings. According to ASHRAE 169 [94], glazing for cities in climate zone 3B consists of two clear glass panes separated by air. For such glazing, the VT, U-value, and SHGC are 0.45, 2.5 W/m^2K, and 0.25, respectively. All HVAC system parameters, internal loads, and operational schedules were defined in accordance with ASHRAE standards (ASHRAE 90.1, ASHRAE 55, and ASHRAE 62.1), ensuring consistency and comparability across all simulated scenarios [95–97].

The specifications of the PV modules are shown in Table 3. The energy generated by the PV modules, the electrical energy consumption, and energy savings were calculated for the sample room using the OpenStudio engine version 0.0.66. The two modes, ASOF and AMOF, were used in the simulation to compare the energy generated at different angles of the PV modules.

3. Results

This section presents the simulation outputs for two adaptive solar façade systems, Adaptive Single-objective Optimization Façade (ASOF) and Adaptive Multi-objective Optimization Façade (AMOF), installed on a south-facing office building in Tehran, Iran. The performance assessment considered two primary domains: visual comfort, evaluated by Useful Daylight Illuminance (UDI) and Daylight Glare Probability (DGP); and energy performance, including photovoltaic electricity generation and net energy use (lighting, heating, cooling, and equipment). Nine Hours of the Year (HOYs) were simulated, taken from March 21, September 21, and December 21, in accordance with LEED v4 recommendations.

The building was exposed to a “Sunny with Sun” CIE standard sky condition (Table 5). Results are compared to a baseline case with an unshaded window. All comparative energy performance results are calculated relative to a baseline case representing the same office room without any photovoltaic façade or external shading. The baseline and all ASF scenarios were simulated using identical weather files, occupancy schedules, internal loads, HVAC system type, thermostat setpoints, infiltration rates, and simulation timesteps. Façade configurations were optimized using the Octopus genetic algorithm, with simulations run in Honeybee and EnergyPlus via Grasshopper. Accurate rendering settings ensured high-fidelity data, enabling robust multi-criteria analysis.

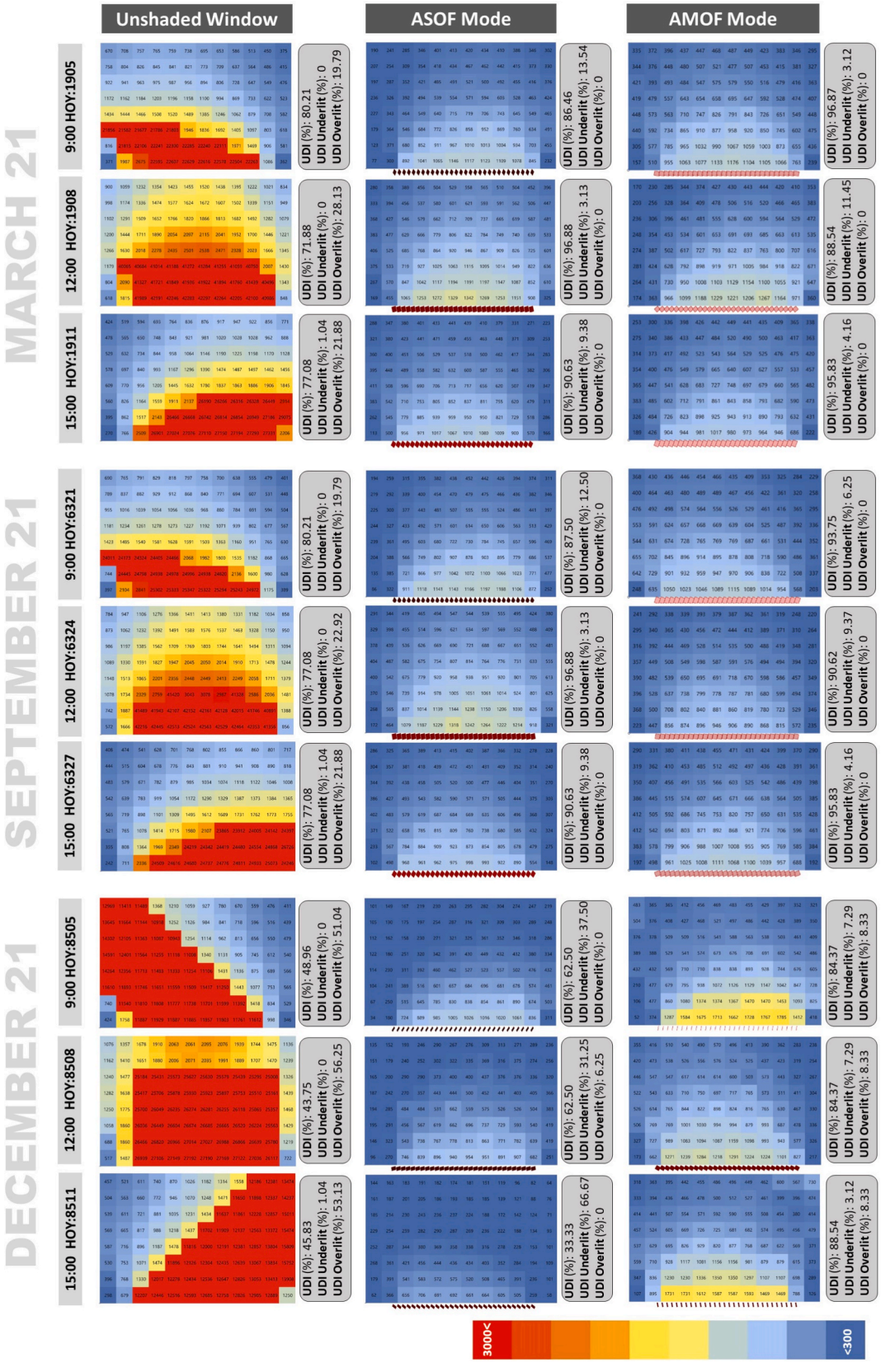

Fig. 13. Hourly daylight illuminance in three different modes.

Table 7
Comparison of the DGP and GCR results in three different modes.

	HOY	Unshaded window DGP			(ASOF) Mode DGP			(AMOF) Mode DGP		
		1	2	3	1	2	3	1	2	3
March 21	1905	0.42[c]	0.23[a]	0.60[d]	0.33[a]	0.21[a]	0.26[a]	0.34[a]	0.21[a]	0.26[a]
	1908	0.71[d]	0.28[a]	0.60[d]	0.37[b]	0.22[a]	0.29[a]	0.34[a]	0.22[a]	0.29[a]
	1911	0.63[d]	0.50[d]	0.28[a]	0.33[a]	0.21[a]	0.29[a]	0.33[a]	0.20[a]	0.29[a]
September 21	6321	0.44[c]	0.23[a]	0.60[d]	0.34[a]	0.22[a]	0.27[a]	0.34[a]	0.21[a]	0.27[a]
	6324	0.71[d]	0.27[a]	0.38[b]	0.41[c]	0.20[a]	0.29[a]	0.32[a]	0.22[a]	0.29[a]
	6327	0.46[d]	0.50[d]	0.28[a]	0.32[a]	0.20[a]	0.29[a]	0.34[a]	0.20[a]	0.28[a]
December 21	8505	1.00[d]	0.29[a]	1.00[d]	0.29[a]	0.20[a]	0.24[a]	0.34[a]	0.20[a]	0.24[a]
	8508	1.00[d]	0.35[b]	0.40[c]	0.31[a]	0.20[a]	0.25[a]	0.34[a]	0.20[a]	0.25[a]
	8511	1.00[d]	1.00[d]	0.27[a]	0.26[a]	0.13[a]	0.24[a]	0.34[a]	0.13[a]	0.24[a]
	GCR	a)imperceptible		b)perceptible		c)disturbing		d)intolerable		

3.1. Optimization dataset and simulation setup

Adaptive façade configurations were parametrically generated based on nine vertical and eighteen horizontal PV module angles across nine HOYs. The AMOF mode is simultaneously optimized for visual comfort, defined by a UDI of 300–3,000 lx and a DGP below 0.35, and for solar energy production. In contrast, ASOF relied on sun-tracking via photocell sensors to maximize incident radiation, without considering visual comfort metrics.

A web-based tool ("Design Explorer") facilitated the exploration and visualization of trade-offs between Pareto-optimal solutions, while GA outputs were recorded and organized in Microsoft Excel. Visual correlations among design parameters and performance indicators are presented in Fig. 9. The analysis focused on three performance objectives: (i) daylight adequacy across three UDI domains (UDI, $UDI_{overlit}$, $UDI_{underlit}$), (ii) glare metrics across multiple view angles, and (iii) total incident solar radiation on PV surfaces. These indicators formed the basis for quantifying and comparing façade performance.

Fig. 10 illustrates the distribution of solutions within the three-objective optimization space. The optimization assigned equal importance to (i) maximizing UDI ($\geq$75% of the task area receiving 300–3000 lx), (ii) minimizing DGP ($<$0.35), and (iii) maximizing solar irradiance on PV surfaces. The Pareto-based approach revealed clear trade-offs among the objectives: maximizing PV irradiance often required orientations that allowed direct radiation entry, increasing DGP above 0.35 and risking glare, while prioritizing DGP $<$ 0.35 typically resulted in reduced UDI $>$ 75% through greater shading and reduced energy yield.

The selected configurations for each HOY are illustrated in Fig. 11, along with the corresponding PV module angles in AMOF mode. These represent the most balanced trade-offs across performance goals.

3.2. Visual Comfort: UDI and DGP

Visual comfort was evaluated using two industry-standard metrics:

- Useful Daylight Illuminance (UDI): The percentage of the task plane (70 cm above floor level) receiving illuminance between 300 and 3,000 lx across at least 75% of the area.
- Daylight Glare Probability (DGP): Evaluated in three viewing directions — toward outdoor, 45° toward outdoor, and front view—with values below 0.35 signifying imperceptible glare (Fig. 7).

3.2.1. UDI performance

Table 6 presents UDI results for the three façade scenarios. The baseline unshaded window showed erratic performance, with frequent under- or over-lighting. For instance, in winter (HOY 8505), UDI was only 48.96%, while $UDI_{overlit}$ exceeded 50%, resulting in visual discomfort. In contrast, both ASOF and AMOF significantly improved daylight distribution. AMOF demonstrated superior adaptability across all seasons:

- March 21: UDI exceeded 86% for both systems; AMOF reached 96.87% (HOY 1905), highlighting its strength under high solar angles.
- September 21: AMOF maintained UDI above 90%; ASOF ranged between 87% and 96%.
- December 21: ASOF dropped to 33.33% UDI (HOY 8511) as it prioritized energy collection over comfort, leaving 66.67% of the space underlit. Conversely, AMOF sustained UDI above 88%, effectively adapting to low winter sun angles (Fig. 12).

Hourly illuminance patterns (Fig. 13) confirm that AMOF consistently delivered acceptable light levels while minimizing over- and under-lit zones. ASOF, particularly in winter, occasionally led to $UDI_{underlit}$ conditions due to its single-objective optimization.

3.2.2. DGP performance

Daylight Glare Probability (DGP) analysis was conducted for three standard occupant view angles to assess glare discomfort. In the unshaded window condition, DGP values frequently exceeded 0.45, which is categorized as 'intolerable', particularly in March (e.g., HOY 1908: DGP = 0.71) and December (e.g., HOY 8511: DGP = 1.00). Both ASOF and AMOF significantly reduced DGP across all views, often maintaining values below the imperceptible threshold of 0.35 (Table 7).

AMOF consistently outperformed ASOF in maintaining glare-free conditions. For example, in September, ASOF reached a DGP of 0.41 at HOY 6324, just above the comfort threshold, whereas AMOF remained below 0.32 across all views. This stability is attributed to AMOF's multi-objective optimization, which inherently balances energy and comfort performance throughout the year. Fig. 14 illustrates DGP results across the three angles, reaffirming AMOF's superiority in mitigating glare, especially in glare-prone periods such as early spring and late autumn.

In addition to glare control, the AMOF also improved visual transparency. Fig. 15 addresses a common concern in Building-Integrated Photovoltaics (BIPV): obstructed views. In AMOF mode, the PV modules are angled to maintain outdoor visibility while harvesting solar energy. The white areas in the figure represent transparent zones with unobstructed views, while the black areas indicate opaque PV surfaces. Compared to ASOF, AMOF consistently offered broader view openings due to its wider-angle configurations (especially in winter), enhancing occupant connection to the outdoor environment.

3.3. Energy Performance: Generation and consumption

Energy performance was evaluated by analyzing both the electricity generated by the PV-integrated façade systems and the total energy consumed by the office room across the nine HOYs. This dual assessment helps capture the trade-offs between energy production and building energy demand. Fig. 16 presents the comparison between generation

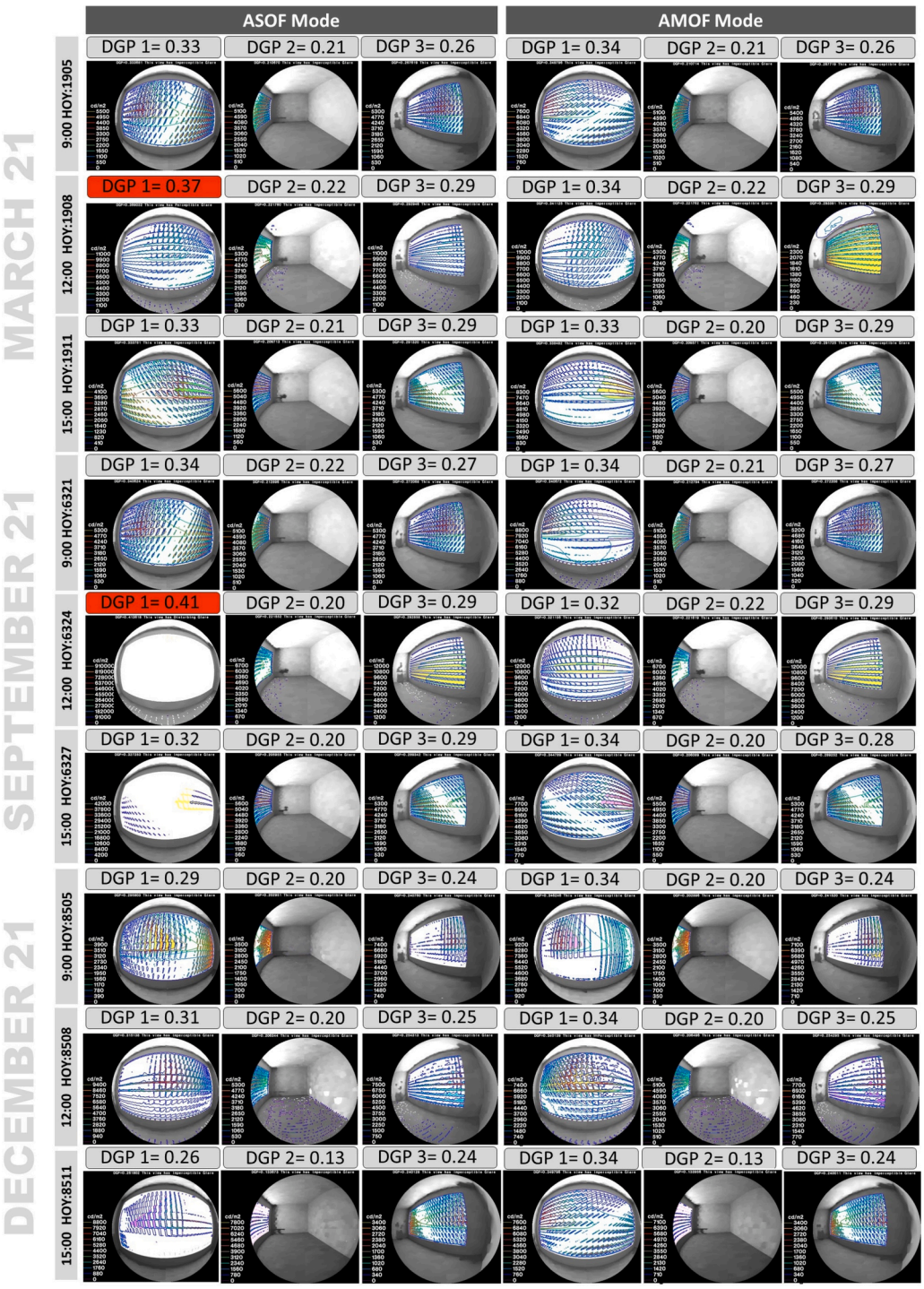

Fig. 14. Glare probability of three different view.

and use across the ASOF, AMOF, and unshaded window conditions.

3.3.1. *Electricity generation*

The electricity generation analysis focused on total incident solar radiation on the PV surfaces; Fig. 17 illustrates the impact of shading on PV cell energy production. According to the explanations previously provided in Section 2.4, based on the efficiency of the amorphous-silicon solar cell used in this study, approximately 10% of this amount can be utilized. ASOF, which is optimized solely for solar tracking, consistently outperformed AMOF across electricity generation metrics.

- March 21: ASOF generated 0.79 kWh versus AMOF's 0.74 kWh.
- September 21: ASOF achieved 0.62 kWh, compared to 0.60 kWh for AMOF.
- December 21: ASOF produced 0.46 kWh, while AMOF reached 0.38 kWh.

Despite this, AMOF still met 68.53% of the room's energy needs, while ASOF covered 75.10% (see Table 8). These results underline AMOF's deliberate trade-off, prioritizing visual comfort while maintaining a high level of energy self-sufficiency. Hourly total radiation falling on PV surfaces on nine selected HOYs is shown in Fig. 18.

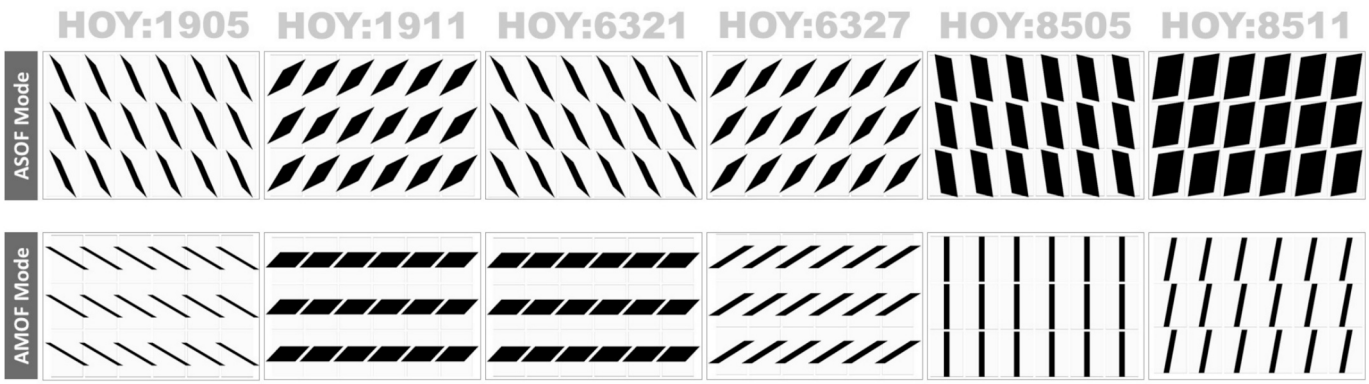

Fig. 15. ASOF vs. AMOF modes in terms of transparency. The black surface is composed of PV opaque material that lacks transparency, while the white space represents areas where users can see outside.

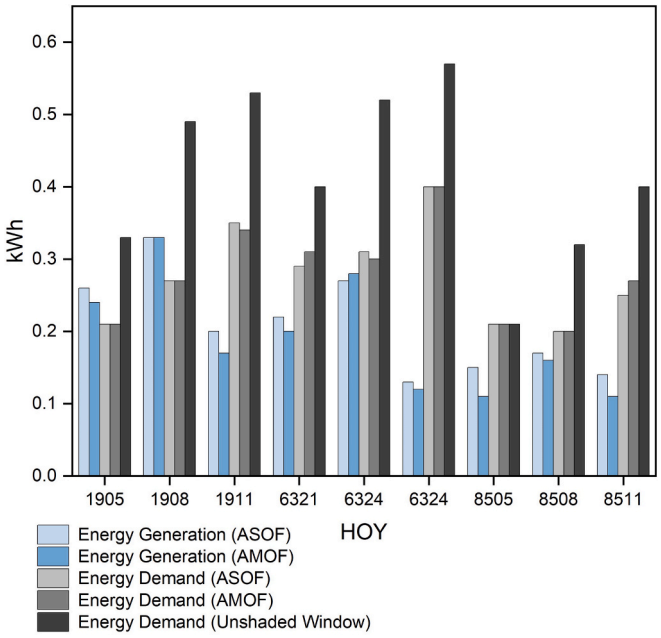

Fig. 16. Comparison between energy generation and use for ASOF, AMOF, and the baseline condition.

3.3.2. *Electricity consumption*

Across the nine HOYs, the total energy use of the baseline (unshaded window) condition was 3.77 kWh, primarily driven by elevated cooling and lighting loads. In contrast, the ASOF and AMOF systems significantly lowered total use to 2.49 kWh and 2.51 kWh, respectively, representing reductions of 33.95% and 33.42% (Table 8). Compared to the unshaded baseline case under identical simulation assumptions, both ASF configurations reduced total energy use by approximately 33%, with differences arising solely from the façade control strategy.

The performance gap between ASOF and AMOF is negligible, indicating that the enhanced comfort provided by AMOF did not result in a substantial energy penalty. Moreover, both systems were capable of exceeding the hourly demand during peak solar periods (e.g., HOY 1908), resulting in temporary net-positive energy balances (Figs. 19 and 20).

To contextualize the electricity use results, an estimate for the energy consumption of the servo motors was conducted. Each dual-axis PV module of the prototype contains two servo motors with an average operating power of 5 W during active adjustment [98].

Under a conservative dynamic usage scenario of 90 s of movement per day, the active runtime of the servo motors would amount to 6.5 h per year; this equates to 0.033 kWh/year per module. For a facade array consisting of 300 modules, the total actuator consumption would be ~ 9.9 kWh/year, approximately 1.5% of the annual PV generation (depending on solar radiation levels). These results align with actuator consumption ranges reported by Ozadowicz and Walczyk (2023), which supports that when movement frequency is minimized through effective control strategies, the energy penalty from actuation is minimal [99].

4. Validation and discussion

4.1. *Validation of PV output*

The validation focused on measuring PV electricity output from an experimental prototype with 14 amorphous-silicon (a-Si) PV modules (each 0.2 m × 0.14 m, nominal efficiency 8–10%), tested in Tehran from December 12 to 21, 2024, at 9:00, 12:00, and 15:00 daily (30 measurements total). Instantaneous PV power output (in W) was measured using an Arduino-based energy meter (Fig. 21), comprising a Talema AC1030 current transformer (turns ratio 1000:1, primary current 30 A, ratio error 0% at 48 Ω load), a 10 μF capacitor for signal stabilization, and precision resistors (56 Ω and a 2 × 100 kΩ voltage divider). Measured power outputs were compared to Honeybee simulations under identical on-site conditions. The correlation yielded $R^2 = 0.8251$ (Fig. 22), mainly attributable to unmodeled factors like module temperature fluctuations (±2–5 °C) and dust effects. This empirical validation affirms the simulation's accuracy for PV power performance in semi-arid environments. Additionally, actuator performance was monitored during prototype operation to ensure correct rotational behavior.

While visual comfort metrics, such as UDI and DGP, were primarily derived from simulations using validated Radiance and Daysim engines, data from the PV system and actuators provide indirect validation by confirming the accuracy of the environmental and mechanical models used. The details of the programming and coding of the modules lie beyond the scope of this paper.

4.2. *Discussion*

This article evaluates an office in Tehran that uses the Adaptive Solar Façade (ASF) system, comparing it with the Adaptive Single-objective Optimization Façade (ASOF) and the Adaptive Multi-objective Optimization Façade (AMOF). It utilizes photovoltaic (PV) façades, employs parametric design tools, and integrates multi-objective optimization to bridge gaps in the literature by evaluating adaptive energy systems for both visual comfort and energy efficiency.

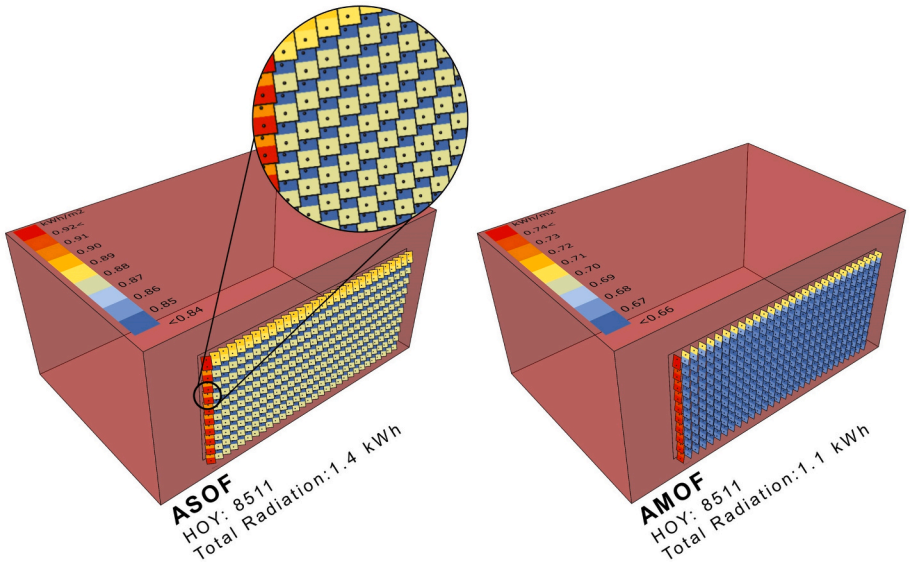

Fig. 17. Hourly incident radiation on PV surfaces for HOY 8511. Dual test points per PV module improve shading accuracy.

Table 8
Comparison between energy generation and use.

HOY		ASOF		AMOF		Unshaded Window	
		Energy Generation (kWh)	Energy Consumption (kWh)	Energy Generation (kWh)	Energy Consumption (kWh)	Energy Generation (kWh)	Energy Consumption (kWh)
March 21	1905	0.26	0.21	0.24	0.21	0	0.33
	1908	0.33	0.27	0.33	0.27	0	0.49
	1911	0.2	0.35	0.17	0.34	0	0.53
September 21	6321	0.22	0.29	0.2	0.31	0	0.4
	6324	0.27	0.31	0.28	0.3	0	0.52
	6327	0.13	0.4	0.12	0.4	0	0.57
December 21	8505	0.15	0.21	0.11	0.21	0	0.21
	8508	0.17	0.2	0.16	0.2	0	0.32
	8511	0.14	0.25	0.11	0.27	0	0.4
Total (kWh)		**1.87**	**2.49**	**1.72**	**2.51**	0	**3.77**
Room energy supply (%)		**75.10**		**68.53**			
Energy saving in comparison with unshaded condition (%)		**33.95**		**33.42**			

4.2.1. Performance Comparison: ASOF vs. AMOF

The ASOF configuration, designed to maximize energy output by optimizing PV module positioning, produced more energy than the AMOF configuration, which met 68.53% of overall demand. In contrast, ASOF met 75.10% of demand. However, this came at the expense of visual comfort, particularly in December, when the UDI threshold was not met and over 66.67% of the task plane fell into the $UDI_{underlit}$ domain (HOY 8511). On the other hand, AMOF, which simultaneously optimizes UDI, Daylight Glare Probability (DGP), and solar radiation control, maintained UDI above 75% and DGP below 0.35, even under challenging conditions such as December 21. For instance, at HOY 8511, AMOF improved UDI to 88.54%, compared to 33.33% in ASOF mode, while still generating 40% of the energy demand. Moreover, glare analysis indicates that AMOF controls DGP to imperceptible levels, thereby improving outdoor visibility, a criticism often raised against dynamic façades (Fig. 15).

4.2.2. Energy efficiency and generation Perspectives

Energy analysis showed that both systems outperformed the unshaded baseline by up to 34% in energy usage over nine selected hours. Although ASOF produces more energy, 0.79 kWh compared to 0.74 kWh on March 21, AMOF's integrated approach compensates with better energy savings and visual comfort. The seasonal variation in performance is also noteworthy. Due to favorable sun angles, March and September showed higher energy generation, whereas December had lower loading output due to decreased solar availability. However, AMOF's capacity to adapt to these changes highlights its year-round efficacy, in contrast to ASOF, which struggles during winter due to reduced daylight. This feature confirms the findings of Nagy et al. (2016) on the benefits of two-axis solar tracking. It extends their research on visual comfort, making AMOF a more robust solution for areas with significant seasonal fluctuations. During peak solar hours (e.g., HOY 1908), energy production exceeds consumption. This suggests that surplus energy can be stored in batteries, thereby increasing overall efficiency. This aligns with findings from Jayathissa et al. (2017), who reported net energy savings of 20–80% with dynamic BIPV shading; however, their study omitted visual comfort optimization, a gap addressed in this research.

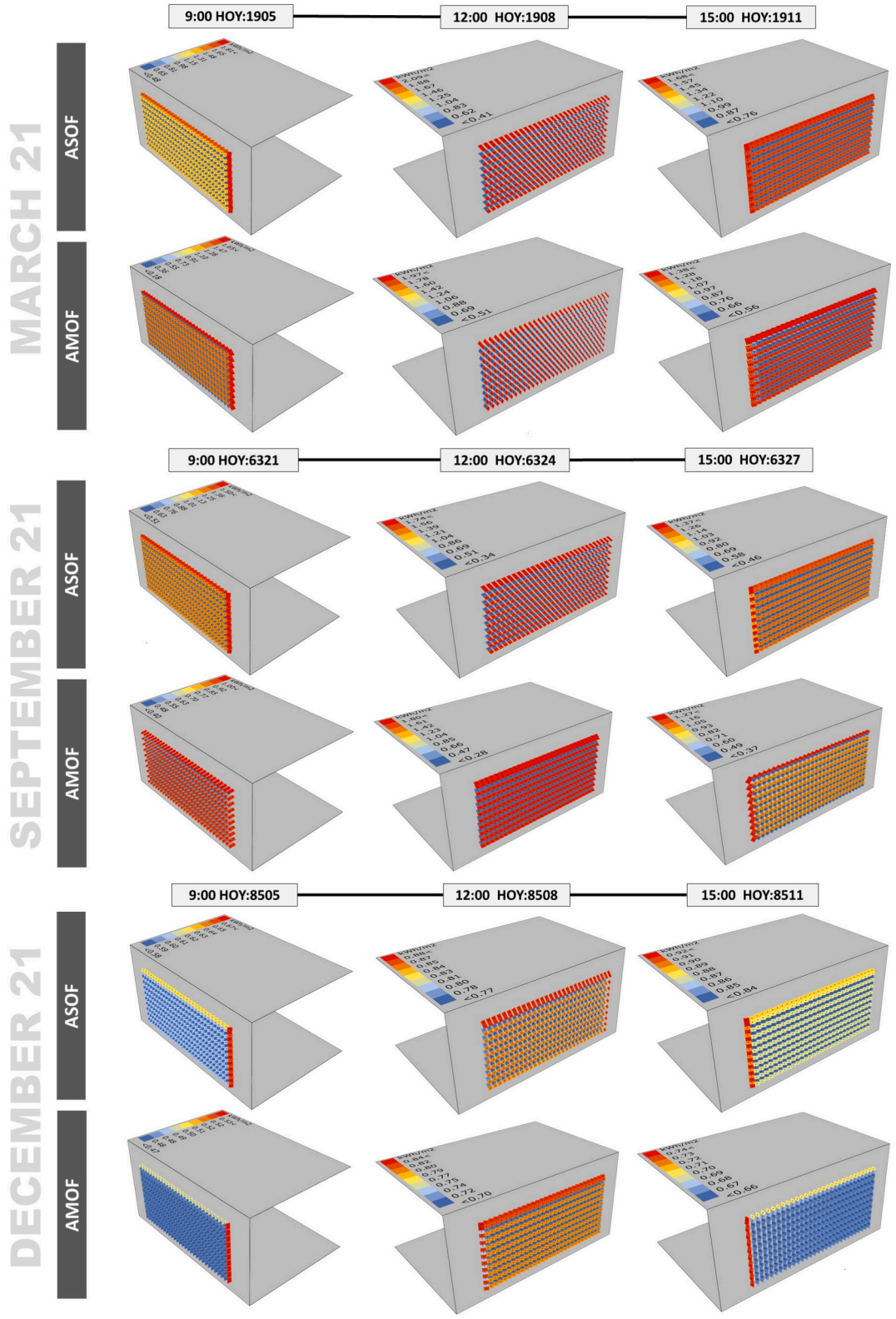

Fig. 18. Hourly total radiation on PV surfaces across nine HOYs.

4.2.3. Validation and reliability

The study's credibility is further enhanced by validating it with current data. The simulation results showed satisfactory agreement with the PV generation data, with an R-squared value of 0.8251. The data collected during 10 days in December 2024 helped bridge the gap between simulation and practical data. This verified the accuracy of the simulation data and addressed a limitation noted in prior studies, such as Rizi and Eltaweel (2021), which relied solely on simulation data.

The present study does not explicitly quantify actuator energy consumption or long-term mechanical durability; while expected to be minor relative to operational energy savings, these aspects should be assessed through long-term monitoring and lifecycle maintenance

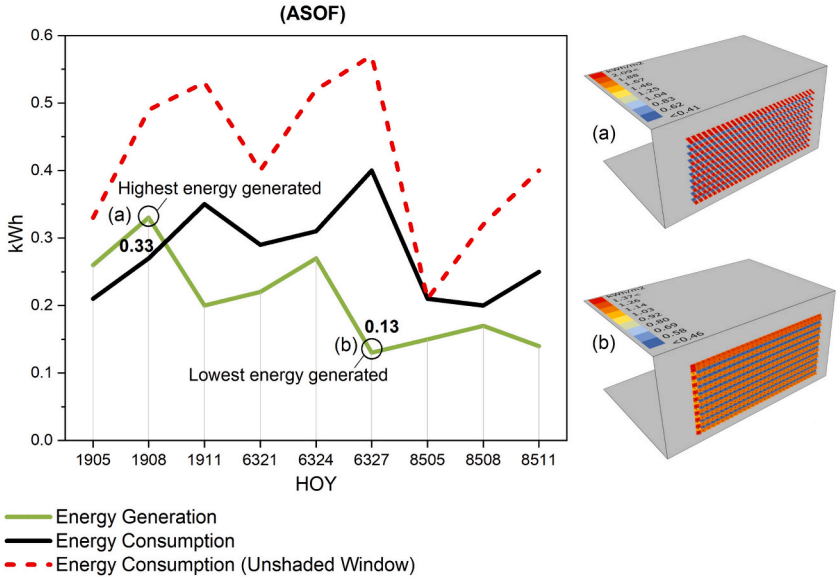

Fig. 19. Hourly energy generation and use for nine HOYs – ASOF.

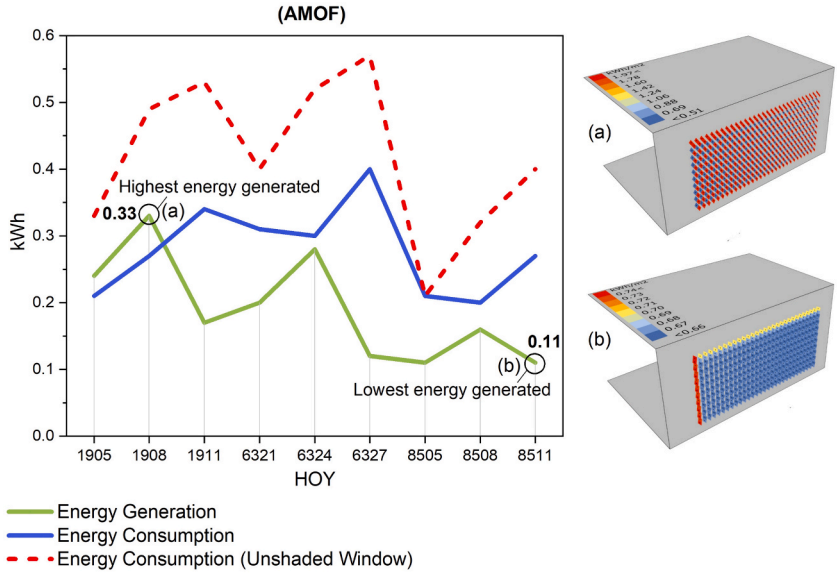

Fig. 20. Hourly energy generation and use for nine HOYs – AMOF.

analysis in future work.

4.2.4. Impact of occupant behavior

A critical yet underexplored aspect of façade performance is the influence of occupant behavior, which introduces real-world variability not fully captured by the controlled simulations in this article. In reality, building occupants could control the automation (e.g., by moving a joystick), thereby disrupting the optimal balance among UDI, DGP, and energy generation. For example, reduced glare or increased solar gain resulting from manually intended adjustments to enhance outdoor views can lower the 33.95% energy-saving simulation results. This emphasizes the need for more research that provides real-time user feedback to understand the trade-offs between user comfort and system performance.

4.2.5. Broader Implications: Costs, Maintenance, and failure points

The adaptive solar systems discussed in this paper have significant potential for sustainable urbanism and decarbonization in Tehran, where solar irradiation potential is substantial and cooling demand is high. The AMOF and ASOF systems possess significant energy and comfort benefits. However, the practical implications for costs and ongoing operating factors, such as installation, maintenance, and potential failure risks, require further evaluation.

The dual-axis servo motors for real-time adjustment of the PV modules each cost about $20–50, thereby requiring additional initial capital costs compared to static façades. During operation, each motor consumes 3–5 W, a small amount that could slightly reduce net energy yield with frequent repositioning. Maintenance emerges as a key hurdle, with mechanical parts requiring routine servicing, exacerbated by Tehran's dusty, semi-arid climate. For broader deployment, these adaptive BIPV systems cost around 255–2500 €/m2, with the kinetic parts adding another 20–50% to the cost due to the actuators and controls [100,101]. A UK study estimated the average cost of a fully installed 2.1 kWp BIPV system at £10,500 to £13,150, but costs can be higher for complex designs [102]. Regular maintenance, such as oiling parts and removing dust, can increase annual costs, which aligns with

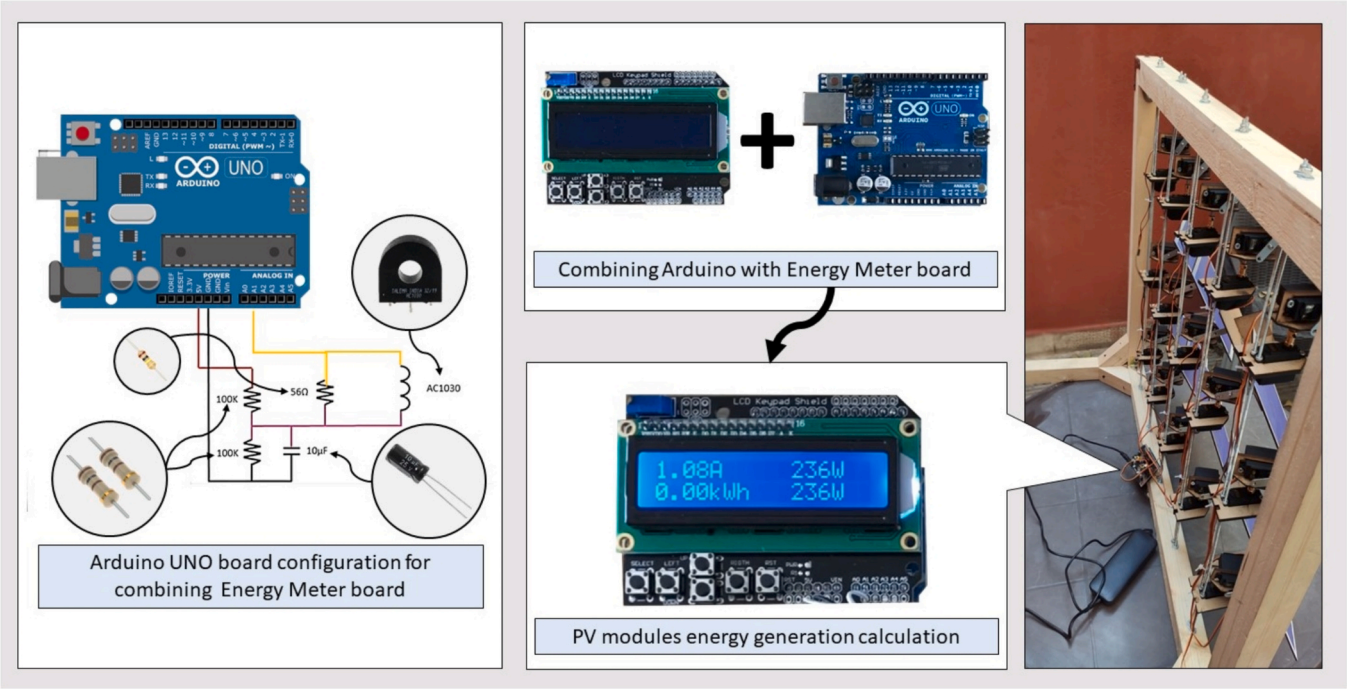

Fig. 21. Experimental setup: (Left) Arduino energy meter board; (Middle) energy meter board assembly; (Right) full prototype installation.

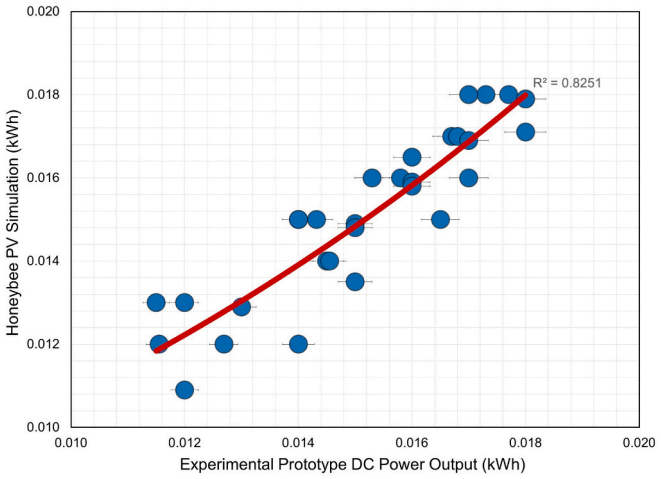

Fig. 22. Validation plot showing correlation ($R^2 = 0.8251$) between simulated and measured PV output.

findings on the challenges associated with BIPV systems and the necessity for inspections [103]. Failure risks include actuator fatigue after 5–10 years, PV module electrical issues, or inverter breakdowns [104]. Despite static alternatives incurring much lower costs, the systems' savings of 20–40% on energy expenses could amortize the system's cost, justifying lifecycle evaluations for larger-scale feasibility in incentivized renewable areas [105,106].

4.2.6. *Recommendations for practitioners*

In the process of adapting systems for effective use within hot and semi-arid climates, practitioners may choose to further carry out the following tasks with parametric software and AMOF systems such as Grasshopper and Honeybee: First, site-specific solar radiation and daylighting research to determine baseline conditions; Second, a PV façade stage that employs two-axis servo motors and permits higher degrees of freedom; Third, control systems modifications that include multi-objective optimization for UDI, DGP, and sufficiency of energy generation; and last, user interfaces (i.e., joystick controls) allowing the user to adjust controls within their criteria. Energy storage devices, such as batteries, should also be integrated with PV systems to capture surplus energy generated during peak periods. In the dusty conditions of cities such as Tehran, actuators and PV modules must be serviced regularly.

4.2.7. *Future research directions*

Several directions need more research. Firstly, a machine learning technique could be applied to predictive modeling to enhance double-skin solar façade systems by predicting solar radiation in real time. Secondly, extending the research to other regions, such as humid or temperate ones, would test the system's generalizability and contribute to addressing Nagy et al.'s (2016) challenge regarding the climate scope. Third, hybrid approaches that combine the optimization framework with advanced materials could make BIPV performance even better. Lastly, a wide econometric analysis of the viability of AMOF versus ASOF systems with respect to actuators and maintenance costs would fill the gap identified by Hofer et al. (2016).

Despite the contributions, it is important to recognize the limitations. As indicators covering various potential scenarios across a year, the optimization solutions were applied to the extreme conditions of the nine steps. This method may provide an indication of the prototype's adaptability to other periods, and the authors acknowledge this as an inevitable study limitation. Additionally, the prototype validation was performed only in winter conditions; validating across multiple seasons would further enhance robustness. Therefore, further evaluation is needed for different conditions, which could be addressed in a future article.

5. Conclusion

The core contribution of this work is the direct comparison of the Adaptive Multi-objective Optimization Façade (AMOF) and Adaptive Single-objective Optimization Façade (ASOF) optimization strategies, demonstrating that multi-objective approaches resolve energy-comfort trade-offs with negligible penalties (e.g., ~0.5% energy loss for DGP

< 0.35 and hUDI > 75%). By integrating DGP as an objective, AMOF ensures superior visual comfort in semi-arid climates, where glare from intense direct radiation is a primary challenge. Simulation and experimental validation results indicate that, though ASOF generates slightly more energy (75.1% of demand vs. 68.5% for AMOF), visual comfort during the winter period is compromised. Conversely, AMOF consistently maintains Useful Daylight Illuminance (UDI) above 75% and Daylight Glare Probability (DGP) below 0.35 across all HOYs, ensuring glare-free, well-lit interior zones and still attaining considerable energy savings (33.4% reduction compared to an unshaded window). The results confirm that multi-objective optimization increases the responsiveness of PV façades in balancing daylight, glare, and energy trade-offs. The inclusion of experimental validation ($R^2 = 0.8251$) further supports the reliability of the simulation-based performance claims.

These results provide actionable recommendations for engineers and architects developing next-generation façades in solar-rich regions. Future work should extend to whole-building applications, climate-based control strategies, long-term monitoring, and cost-benefit analysis of actuator systems to facilitate broader implementation of adaptive solar envelopes.

CRediT authorship contribution statement

Mohsen Zibaraftar: Writing – review & editing, Writing – original draft, Visualization, Validation, Software, Resources, Project administration, Methodology, Formal analysis, Data curation, Conceptualization. **Ahmadreza Khalili:** Validation, Software, Methodology, Investigation. **Shady Attia:** Writing – review & editing, Supervision, Investigation.

Declaration of Competing Interest

The authors declare that they have no known competing financial interests or personal relationships that could have appeared to influence the work reported in this paper.

Acknowledgments

AI language models were used exclusively for editorial purposes, including grammar correction and readability improvements. All scientific content, analyses, and interpretations were generated entirely by the authors.

Appendix A. Supplementary data

Supplementary data to this article can be found online at https://doi.org/10.1016/j.solener.2026.114761.

Data availability

Data are contained within the article.

References

[1] D.H.W. Li, S.K.H. Chow, E.W.M. Lee, An analysis of a medium size grid-connected building integrated photovoltaic (BIPV) system using measured data, Energy Build. 60 (May 2013) 383–387, https://doi.org/10.1016/j.enbuild.2013.02.007.
[2] M. Abdolzadeh, M. Sadeqkhani, A. Ahmadi, Computational modeling of a BIPV/T ethylene tetrafluoroethylen (ETFE) cushion structure roof, Energy 133 (Aug. 2017) 998–1012, https://doi.org/10.1016/j.energy.2017.05.144.
[3] E. Marshall, J.K. Steinberger, V. Dupont, T.J. Foxon, Combining energy efficiency measure approaches and occupancy patterns in building modelling in the UK residential context, Energy Build. 111 (Jan. 2016) 98–108, https://doi.org/10.1016/j.enbuild.2015.11.039.
[4] J. de S. Freitas, J. Cronemberger, R. M. Soares, and C. N. D. Amorim, "Modeling and assessing BIPV envelopes using parametric Rhinoceros plugins Grasshopper and Ladybug," *Renew. Energy*, vol. 160, pp. 1468–1479, Nov. 2020, doi: 10.1016/j.renene.2020.05.137.
[5] N. Novas, R.M. Garcia, J.M. Camacho, A. Alcayde, Advances in Solar Energy towards Efficient and Sustainable Energy, Sustainability 13 (11) (Jun. 2021) 6295, https://doi.org/10.3390/su13116295.
[6] T. Mendis, Z. Huang, S. Xu, W. Zhang, Economic potential analysis of photovoltaic integrated shading strategies on commercial building facades in urban blocks: a case study of Colombo, Sri Lanka, Energy 194 (Mar. 2020) 116908, https://doi.org/10.1016/j.energy.2020.116908.
[7] M. Konstantoglou, A. Tsangrassoulis, Dynamic operation of daylighting and shading systems: a literature review, Renew. Sustain. Energy Rev. 60 (Jul. 2016) 268–283, https://doi.org/10.1016/j.rser.2015.12.246.
[8] A. Sharma, A comprehensive study of solar power in India and World, Renew. Sustain. Energy Rev. 15 (4) (May 2011) 1767–1776, https://doi.org/10.1016/j.rser.2010.12.017.
[9] S. Mekhilef, S.Z. Faramarzi, R. Saidur, Z. Salam, The application of solar technologies for sustainable development of agricultural sector, Renew. Sustain. Energy Rev. 18 (Feb. 2013) 583–594, https://doi.org/10.1016/j.rser.2012.10.049.
[10] A. Buonomano, F. Calise, A. Palombo, M. Vicidomini, BIPVT systems for residential applications: an energy and economic analysis for European climates, Appl. Energy 184 (Dec. 2016) 1411–1431, https://doi.org/10.1016/j.apenergy.2016.02.145.
[11] S. Shafiei, R.A. Salim, Non-renewable and renewable energy consumption and CO2 emissions in OECD countries: a comparative analysis, Energy Policy 66 (Mar. 2014) 547–556, https://doi.org/10.1016/j.enpol.2013.10.064.
[12] A. Strzalka, N. Alam, E. Duminil, V. Coors, U. Eicker, Large scale integration of photovoltaics in cities, Appl. Energy 93 (May 2012) 413–421, https://doi.org/10.1016/j.apenergy.2011.12.033.
[13] D. Assouline, N. Mohajeri, J.-L. Scartezzini, Quantifying rooftop photovoltaic solar energy potential: a machine learning approach, Sol. Energy 141 (Jan. 2017) 278–296, https://doi.org/10.1016/j.solener.2016.11.045.
[14] H. Gholami, H.N. Røstvik, D. Müller-Eie, Holistic economic analysis of building integrated photovoltaics (BIPV) system: Case studies evaluation, Energy Build. 203 (Nov. 2019) 109461, https://doi.org/10.1016/j.enbuild.2019.109461.
[15] J.Y. Suk, Luminance and vertical eye illuminance thresholds for occupants' visual comfort in daylit office environments, Build. Environ. 148 (Jan. 2019) 107–115, https://doi.org/10.1016/j.buildenv.2018.10.058.
[16] J. Wienold, J. Christoffersen, Evaluation methods and development of a new glare prediction model for daylight environments with the use of CCD cameras, Energy Build. 38 (7) (Jul. 2006) 743–757, https://doi.org/10.1016/j.enbuild.2006.03.017.
[17] D. Powell, I. Hischier, P. Jayathissa, B. Svetozarevic, A. Schlüter, A reflective adaptive solar façade for multi-building energy and comfort management, Energy Build. 177 (Oct. 2018) 303–315, https://doi.org/10.1016/j.enbuild.2018.07.040.
[18] S. Attia, S. Bilir, T. Safy, C. Struck, R. Loonen, F. Goia, Current trends and future challenges in the performance assessment of adaptive façade systems, Energy Build. 179 (Nov. 2018) 165–182, https://doi.org/10.1016/j.enbuild.2018.09.017.
[19] P. Littlefair, J. Ortiz, and C. Das Bhaumik, "A simulation of solar shading control on UK office energy use," *Build. Res. Inf.*, vol. 38, no. 6, pp. 638–646, Dec. 2010, doi: 10.1080/09613218.2010.496556.
[20] P. Schumacher, Parametricism: a New Global style for Architecture and Urban Design, Archit. Des. 79 (4) (Jul. 2009) 14–23, https://doi.org/10.1002/ad.912.
[21] Y. Fang, S. Cho, Design optimization of building geometry and fenestration for daylighting and energy performance, Sol. Energy 191 (Oct. 2019) 7–18, https://doi.org/10.1016/j.solener.2019.08.039.
[22] A. Toutou, M. Fikry, W. Mohamed, The parametric based optimization framework daylighting and energy performance in residential buildings in hot arid zone, Alexandria Eng. J. 57 (4) (Dec. 2018) 3595–3608, https://doi.org/10.1016/j.aej.2018.04.006.
[23] E. Taveres-Cachat, G. Lobaccaro, F. Goia, G. Chaudhary, A methodology to improve the performance of PV integrated shading devices using multi-objective optimization, Appl. Energy 247 (Aug. 2019) 731–744, https://doi.org/10.1016/j.apenergy.2019.04.033.
[24] H. Duan, Y. Dong, Q. Ji, Multi-objective optimization of windows and PV louvers on the south façade for cold-region office buildings using machine learning and NSGA-II, Build. Environ. 288 (Jan. 2026) 113984, https://doi.org/10.1016/j.buildenv.2025.113984.
[25] J. Samimi, Estimation of height-dependent solar irradiation and application to the solar climate of Iran, Sol. Energy 52 (5) (May 1994) 401–409, https://doi.org/10.1016/0038-092X(94)90117-K.
[26] P. Alamdari, O. Nematollahi, A.A. Alemrajabi, Solar energy potentials in Iran: a review, Renew. Sustain. Energy Rev. 21 (May 2013) 778–788, https://doi.org/10.1016/j.rser.2012.12.052.
[27] M. Ashjaee, M.R. Roomina, R. Ghafouri-Azar, Estimating direct, diffuse, and global solar radiation for various cities in Iran by two methods and their comparison with the measured data, Sol. Energy 50 (5) (May 1993) 441–446, https://doi.org/10.1016/0038-092X(93)90066-W.
[28] M. Daneshyar, Solar radiation statistics for Iran, Sol. Energy 21 (4) (1978) 345–349, https://doi.org/10.1016/0038-092X(78)90013-0.
[29] G. Najafi, B. Ghobadian, R. Mamat, T. Yusaf, W.H. Azmi, Solar energy in Iran: current state and outlook, Renew. Sustain. Energy Rev. 49 (Sep. 2015) 931–942, https://doi.org/10.1016/j.rser.2015.04.056.
[30] S. Carlucci, F. Causone, F. De Rosa, L. Pagliano, A review of indices for assessing visual comfort with a view to their use in optimization processes to support building integrated design, Renew. Sustain. Energy Rev. 47 (Jul. 2015) 1016–1033, https://doi.org/10.1016/j.rser.2015.03.062.

[31] First Edn. (2010).
[32] P. Chauvel, J.B. Collins, R. Dogniaux, J. Longmore, Glare from windows: current views of the problem, Light. Res. Technol. 14 (1) (Mar. 1982) 31–46, https://doi.org/10.1177/096032718201400103.
[33] A. Tabadkani, M. Valinejad Shoubi, F. Soflaei, and S. Banihashemi, "Integrated parametric design of adaptive facades for user's visual comfort," *Autom. Constr.*, vol. 106, p. 102857, Oct. 2019, doi: 10.1016/j.autcon.2019.102857.
[34] K.A. Kurnia, D.N. Azizah, R.A. Mangkuto, R.T. Atmodipoero, Visual Comfort Assessment using High Dynamic Range Images under Daylight Condition in the Main Library Building of Institut Teknologi Bandung, Procedia Eng. 170 (2017) 234–239, https://doi.org/10.1016/j.proeng.2017.03.056.
[35] D. Hafiz, "Daylighting, Space, and Architecture: A Literature Review," *Enq. ARCC J. Archit. Res.*, vol. 12, no. 1, Dec. 2015, doi: 10.17831/enq:arcc.v12i1.391.
[36] J. Mardaljevic, Simulation of annual daylighting profiles for internal illuminance, Light. Res. Technol. 32 (3) (Jan. 2000) 111–118, https://doi.org/10.1177/096032710003200302.
[37] J. Wienold, Jan; Christoffersen, "Towards a new daylight glare rating," *Proceedinsg Ofthe10thEuropeanLightingConference,LuxEuropa.*, 2005, [Online]. Available: https://www.researchgate.net/publication/313608753_Towards_a_new_daylight_glare_rating.
[38] N.L. Jones, C.F. Reinhart, Experimental validation of ray tracing as a means of image-based visual discomfort prediction, Build. Environ. 113 (Feb. 2017) 131–150, https://doi.org/10.1016/j.buildenv.2016.08.023.
[39] A. Mostafavi, T.B. Xu, S. Kalantari, Effects of illuminance and correlated color temperature on emotional responses and lighting adjustment behaviors, J. Build. Eng. 86 (Jun. 2024) 108833, https://doi.org/10.1016/j.jobe.2024.108833.
[40] Y. Zeng, H. Sun, J. Yu, B. Lin, Effects of correlated color temperature of office light on subjective perception, mood and task performance, Build. Environ. 224 (Oct. 2022) 109508, https://doi.org/10.1016/j.buildenv.2022.109508.
[41] J. Toftum, A. Thorseth, J. Markvart, Á. Logadóttir, Occupant response to different correlated colour temperatures of white LED lighting, Build. Environ. 143 (Oct. 2018) 258–268, https://doi.org/10.1016/j.buildenv.2018.07.013.
[42] H. Xiao, H. Cai, X. Li, Non-visual effects of indoor light environment on humans: a review☆, Physiol. Behav. 228 (Jan. 2021) 113195 https://doi.org/10.1016/j.physbeh.2020.113195.
[43] H. Cai, Q. Lin, H. Liu, X. Li, H. Xiao, Recognition of human mood, alertness and comfort under the influence of indoor lighting using physiological features, Biomed. Signal Process. Control 89 (Mar. 2024) 105661, https://doi.org/10.1016/j.bspc.2023.105661.
[44] S. Shi, Y. Yang, J. Yu, Y. Zeng, B. Lin, Effects of eye illuminance and correlated color temperature on subjective visual comfort, mood, and alertness in high-space buildings, Build. Environ. 283 (Sep. 2025) 113382, https://doi.org/10.1016/j.buildenv.2025.113382.
[45] Y. Zeng, H. Sun, B. Lin, Q. Zhang, Non-visual effects of office light environment: Field evaluation, model comparison, and spectral analysis, Build. Environ. 197 (Jun. 2021) 107859, https://doi.org/10.1016/j.buildenv.2021.107859.
[46] W. Luo, R. Kramer, M. Kompier, K. Smolders, Y. de Kort, and W. van Marken Lichtenbelt, "Effects of correlated color temperature of light on thermal comfort, thermophysiology and cognitive performance," *Build. Environ.*, vol. 231, p. 109944, Mar. 2023, doi: 10.1016/j.buildenv.2022.109944.
[47] Z. Nagy, et al., The Adaptive Solar Facade: from concept to prototypes, Front. Archit. Res. 5 (2) (Jun. 2016) 143–156, https://doi.org/10.1016/j.foar.2016.03.002.
[48] J. Hofer, A. Groenewolt, P. Jayathissa, Z. Nagy, A. Schlueter, Parametric analysis and systems design of dynamic photovoltaic shading modules, Energy Sci. Eng. 4 (2) (Mar. 2016) 134–152, https://doi.org/10.1002/ese3.115.
[49] P. Jayathissa, M. Luzzatto, J. Schmidli, J. Hofer, Z. Nagy, A. Schlueter, Optimising building net energy demand with dynamic BIPV shading, Appl. Energy 202 (Sep. 2017) 726–735, https://doi.org/10.1016/j.apenergy.2017.05.083.
[50] P. Jayathissa, S. Caranovic, J. Hofer, Z. Nagy, A. Schlueter, Performative design environment for kinetic photovoltaic architecture, Autom. Constr. 93 (Sep. 2018) 339–347, https://doi.org/10.1016/j.autcon.2018.05.013.
[51] A. Michael, S. Gregoriou, S.A. Kalogirou, Environmental assessment of an integrated adaptive system for the improvement of indoor visual comfort of existing buildings, Renew. Energy 115 (Jan. 2018) 620–633, https://doi.org/10.1016/j.renene.2017.07.079.
[52] B. Svetozarevic, et al., Dynamic photovoltaic building envelopes for adaptive energy and comfort management, Nat. Energy 4 (8) (Jul. 2019) 671–682, https://doi.org/10.1038/s41560-019-0424-0.
[53] S. D. Sureshkumar Jayakumari *et al.*, "Energy and Daylighting Performance of Kinetic Building-Integrated Photovoltaics (BIPV) Façade," *Sustainability*, vol. 16, no. 22, p. 9739, Nov. 2024, doi: 10.3390/su16229739.
[54] N. Delgarm, B. Sajadi, F. Kowsary, S. Delgarm, Multi-objective optimization of the building energy performance: a simulation-based approach by means of particle swarm optimization (PSO), Appl. Energy 170 (May 2016) 293–303, https://doi.org/10.1016/j.apenergy.2016.02.141.
[55] E. Naderi, B. Sajadi, M.A. Behabadi, E. Naderi, Multi-objective simulation-based optimization of controlled blind specifications to reduce energy consumption, and thermal and visual discomfort: Case studies in Iran, Build. Environ. 169 (Feb. 2020) 106570, https://doi.org/10.1016/j.buildenv.2019.106570.
[56] U. Acar, O. Kaska, N. Tokgoz, Multi-objective optimization of building envelope components at the preliminary design stage for residential buildings in Turkey, J. Build. Eng. 42 (Oct. 2021) 102499, https://doi.org/10.1016/j.jobe.2021.102499.
[57] A. Kirimtat, O. Krejcar, B. Ekici, M. Fatih Tasgetiren, "Multi-objective energy and daylight optimization of amorphous shading devices in buildings", Jun, Sol. Energy 185 (2019) 100–111, https://doi.org/10.1016/j.solener.2019.04.048.
[58] S. Nazari, P. Keshavarz Mirza Mohammadi, and P. Sareh,, A multi-objective optimization approach to designing window and shading systems considering building energy consumption and occupant comfort, Eng. Reports 5 (10) (2023) Oct, https://doi.org/10.1002/eng2.12726.
[59] P. liu *et al.*, "Multi-objective optimization of office building envelopes properties and Venetian blinds using NSGA-II to save energy consumption and enhance thermal and visual comfort," *Case Stud. Therm. Eng.*, vol. 64, p. 105484, Dec. 2024, doi: 10.1016/j.csite.2024.105484.
[60] H. Kim, M.J. Clayton, A multi-objective optimization approach for climate-adaptive building envelope design using parametric behavior maps, Build. Environ. 185 (Nov. 2020) 107292, https://doi.org/10.1016/j.buildenv.2020.107292.
[61] Y. Xu, G. Zhang, C. Yan, G. Wang, Y. Jiang, K. Zhao, A two-stage multi-objective optimization method for envelope and energy generation systems of primary and secondary school teaching buildings in China, Build. Environ. 204 (Oct. 2021) 108142, https://doi.org/10.1016/j.buildenv.2021.108142.
[62] M. Ghaderian, F. Veysi, Multi-objective optimization of energy efficiency and thermal comfort in an existing office building using NSGA-II with fitness approximation: a case study, J. Build. Eng. 41 (Sep. 2021) 102440, https://doi.org/10.1016/j.jobe.2021.102440.
[63] H.H. Hosamo, M.S. Tingstveit, H.K. Nielsen, P.R. Svennevig, K. Svidt, Multiobjective optimization of building energy consumption and thermal comfort based on integrated BIM framework with machine learning-NSGA II, Energy Build. 277 (Dec. 2022) 112479, https://doi.org/10.1016/j.enbuild.2022.112479.
[64] P. Pilechiha, M. Mahdavinejad, F. Pour Rahimian, P. Carnemolla, and S. Seyedzadeh, "Multi-objective optimisation framework for designing office windows: quality of view, daylight and energy efficiency," *Appl. Energy*, vol. 261, p. 114356, Mar. 2020, doi: 10.1016/j.apenergy.2019.114356.
[65] D. Lee, Y.-H. Cho, J.-H. Jo, Assessment of control strategy of adaptive façades for heating, cooling, lighting energy conservation and glare prevention, Energy Build. 235 (Mar. 2021) 110739, https://doi.org/10.1016/j.enbuild.2021.110739.
[66] P. Bakmohammadi, E. Noorzai, Optimization of the design of the primary school classrooms in terms of energy and daylight performance considering occupants' thermal and visual comfort, Energy Rep. 6 (Nov. 2020) 1590–1607, https://doi.org/10.1016/j.egyr.2020.06.008.
[67] R.A. Rizi, A. Eltaweel, A user detective adaptive facade towards improving visual and thermal comfort, J. Build. Eng. 33 (Jan. 2021) 101554, https://doi.org/10.1016/j.jobe.2020.101554.
[68] S. Tharushi Imalka, R. J. Yang, and Y. Zhao, "Machine learning driven building integrated photovoltaic (BIPV) envelope design optimization," *Energy Build.*, vol. 324, p. 114882, Dec. 2024, doi: 10.1016/j.enbuild.2024.114882.
[69] Z. Qi, Z. Wan, L. Li, Q. Ma, W. Gao, X. Wei, Kirigami-inspired novel photovoltaic shading facade: multi-objective optimization of energy consumption, daylighting, thermal comfort, visual comfort, and landscape view, Sol. Energy 299 (Oct. 2025) 113692, https://doi.org/10.1016/j.solener.2025.113692.
[70] Q. Yang, Q. Liu, Y. Du, K. Wang, Integrated design of building envelopes and photovoltaic systems for cold climate office buildings, Sol. Energy 303 (Jan. 2026) 114128, https://doi.org/10.1016/j.solener.2025.114128.
[71] Z. Chen, Y. Cui, H. Cai, H. Zheng, Q. Ning, X. Ding, Multi-objective optimization of photovoltaic facades in prefabricated academic buildings using transfer learning and genetic algorithms, Energy 328 (Aug. 2025) 136470, https://doi.org/10.1016/j.energy.2025.136470.
[72] L. Zhang, A. Alizadeh, M. Baghoolizadeh, S. Salahshour, E. Ali, J. Escorcia-Gutierrez, Multi-objective optimization of vertical and horizontal solar shading in residential buildings to increase power output while reducing yearly electricity usage, Renew. Sustain. Energy Rev. 215 (Jun. 2025) 115578, https://doi.org/10.1016/j.rser.2025.115578.
[73] X. Shi, T. Abel, L. Wang, Influence of two motion types on solar transmittance and daylight performance of dynamic façades, Sol. Energy 201 (May 2020) 561–580, https://doi.org/10.1016/j.solener.2020.03.017.
[74] M.H. Benzaama, S. Menhoudj, M.C. Lekhal, A. Mokhtari, S. Attia, Multi-objective optimisation of a seasonal solar thermal energy storage system combined with an earth – Air heat exchanger for net zero energy building, Sol. Energy 220 (May 2021) 901–913, https://doi.org/10.1016/j.solener.2021.03.070.
[75] S. Singh, S. Agarwal, G.N. Tiwari, D. Chauhan, Application of genetic algorithm with multi-objective function to improve the efficiency of glazed photovoltaic thermal system for New Delhi (India) climatic condition, Sol. Energy 117 (Jul. 2015) 153–166, https://doi.org/10.1016/j.solener.2015.04.025.
[76] E.S. Lee, C. Gehbauer, B.E. Coffey, A. McNeil, M. Stadler, C. Marnay, Integrated control of dynamic facades and distributed energy resources for energy cost minimization in commercial buildings, Sol. Energy 122 (Dec. 2015) 1384–1397, https://doi.org/10.1016/j.solener.2015.11.003.
[77] N. Biloria, M. Makki, N. Abdollahzadeh, Multi-performative façade systems: the case of real-time adaptive BIPV shading systems to enhance energy generation potential and visual comfort, Front. Built Environ. 9 (Mar. 2023), https://doi.org/10.3389/fbuil.2023.1119696.
[78] D. Uribe, S. Vera, W. Bustamante, A. McNeil, G. Flamant, Impact of different control strategies of perforated curved louvers on the visual comfort and energy consumption of office buildings in different climates, Sol. Energy 190 (Sep. 2019) 495–510, https://doi.org/10.1016/j.solener.2019.07.027.
[79] A. Jia, H. Liu, Y. Yun, R. Jiang, S. Pouramini, Energy efficiency measures in existing buildings by a multiple-objective optimization with a solar panel system

using Marine Predators Optimization Algorithm, Sol. Energy 267 (Jan. 2024) 112208, https://doi.org/10.1016/j.solener.2023.112208.
[80] B. Ekici, Z.T. Kazanasmaz, M. Turrin, M.F. Taşgetiren, I.S. Sariyildiz, Multi-zone optimisation of high-rise buildings using artificial intelligence for sustainable metropolises. Part 1: Background, methodology, setup, and machine learning results, Sol. Energy 224 (Aug. 2021) 373–389, https://doi.org/10.1016/j.solener.2021.05.083.
[81] L. Wang, J. Hang, L. Shi, X. Sun, F. Xu, Preparation and characterization of NIR cutoff antimony doped tin oxide/hybrid silica coatings, Mater. Lett. 87 (Nov. 2012) 35–38, https://doi.org/10.1016/j.matlet.2012.07.065.
[82] I. Khele, M. Szabó, A review of the effect of semi-transparent building-integrated photovoltaics on the visual comfort indoors, Dev. Built Environ. 17 (Mar. 2024) 100369, https://doi.org/10.1016/j.dibe.2024.100369.
[83] S. Shi, N. Zhu, Y. Li, Y. Song, Photo-thermal decoupling CdTe PV windows with selectively near-infrared absorbing ATO nanofluids, Renew. Energy 235 (Nov. 2024) 121178, https://doi.org/10.1016/j.renene.2024.121178.
[84] A. Kasaeian, et al., Application of transparent and semi-transparent photovoltaics in building windows: a review, Appl. Energy 405 (Feb. 2026) 127264, https://doi.org/10.1016/j.apenergy.2025.127264.
[85] A.A.F. Husain, W.Z.W. Hasan, S. Shafie, M.N. Hamidon, S.S. Pandey, A review of transparent solar photovoltaic technologies, Renew. Sustain. Energy Rev. 94 (Oct. 2018) 779–791, https://doi.org/10.1016/j.rser.2018.06.031.
[86] B. Petter Jelle, C. Breivik, H. Drolsum Røkenes, "Building integrated photovoltaic products: a state-of-the-art review and future research opportunities", May, Sol. Energy Mater. Sol. Cells 100 (2012) 69–96, https://doi.org/10.1016/j.solmat.2011.12.016.
[87] J. Pu, C. Shen, L. Lu, Investigating the annual energy-saving and energy-output behaviors of a novel liquid-flow window with spectral regulation of ATO nanofluids, Energy 283 (Nov. 2023) 129111, https://doi.org/10.1016/j.energy.2023.129111.
[88] Y. Xie, T. You, B. Dai, H. Cui, A review of colored building-integrated photovoltaics (BIPV) for building decarbonization: Technological and market perspectives, Renew. Sustain. Energy Rev. 235 (Jul. 2026) 116924, https://doi.org/10.1016/j.rser.2026.116924.
[89] J. H. Nicholas Zambetti, Karl Söderby, "Inter-Integrated Circuit (I2C) Protocol." Accessed: Feb. 02, 2024. [Online]. Available: https://docs.arduino.cc/learn/communication/wire/.
[90] "Daylight Indoor Environmental Quality," USGBC organization. [Online]. Available: https://www.usgbc.org/credits/healthcare/v4-draft/eqc-0.
[91] "EnergyPlus, Weather Data by Location." Accessed: Jan. 20, 2025. [Online]. Available: https://energyplus.net/weather-location/asia_wmo_region_2/IRN/IRN_Tehran-Mehrabad.407540_ITMY.
[92] Accessed: May 12 (2024) [Online]. Available: https://jiangsolar.com/product/1w1-5v-flexible-amorphous-thin-film-solar-panel-manufacturers-small-placa-solar/.
[93] D.A. Chi, D. Moreno, J. Navarro, Correlating daylight availability metric with lighting, heating and cooling energy consumptions, Build. Environ. 132 (Mar. 2018) 170–180, https://doi.org/10.1016/j.buildenv.2018.01.048.
[94] ASHRAE, "ANSI, ASHRAE Standard,, Climatic Data for Building Design, American Society of Heating, Refrigerating and Air-Conditioning Engineers", Atlanta, GA 30329 (169–2013,) 2013.
[95] A. Standard, *Energy standard for buildings except low-rise residential buildings*, vol. 2013. 1999. [Online]. Available: https://scholar.google.com/scholar?q=Energy+standard+for+buildings+except+low-rise+residential+buildings.&hl=en&as_sdt=1,5#0.
[96] ASHRAE, "Thermal environmental conditions for human occupancy," in *ASHRAE Standard*, no. 55, 2013.
[97] ASHRAE, "Standard 62.1-2016, Ventilation and Acceptable Indoor Air Quality," in *The American National Standards Institute (ANSI)*, vol. 2016, 2016. [Online]. Available: https://www.ashrae.org/technical-resources/bookstore/standards-62-1-62-2.
[98] "Servo Motor MG995," Soldered. Accessed: Aug. 15, 2025. [Online]. Available: https://www.mouser.com/catalog/specsheets/Soldered_109042.pdf?srsltid=AfmBOoo0uyALb2R3MBxucKk2sI7JQsT27xYU8iqlyDFytfZ_itt5DKf.
[99] A. Ożadowicz, G. Walczyk, Energy Performance and Control Strategy for Dynamic Façade with Perovskite PV Panels—Technical Analysis and Case Study, Energies 16 (9) (Apr. 2023) 3793, https://doi.org/10.3390/en16093793.
[100] F. Batista, A.S. Guimarães, A.I. Palmero-Marrero, Building Integrated Photovoltaics: a multi-level design review for optimized implementation, Renew. Sustain. Energy Rev. 220 (Sep. 2025) 115837, https://doi.org/10.1016/j.rser.2025.115837.
[101] O. Nwafor, "Integrated Photovoltaic Applications: Technological Advancements, Case Studies, Economic Viability, Policy Implications, and Environmental Impact," *Sol. Compass*, p. 100136, Aug. 2025, doi: 10.1016/j.solcom.2025.100136.
[102] G.P. Hammond, H.A. Harajli, C.I. Jones, A.B. Winnett, Whole systems appraisal of a UK Building Integrated Photovoltaic (BIPV) system: Energy, environmental, and economic evaluations, Energy Policy 40 (Jan. 2012) 219–230, https://doi.org/10.1016/j.enpol.2011.09.048.
[103] K. Kumba, P. Upender, P. Buduma, M. Sarkar, S.P. Simon, V. Gundu, Solar tracking systems: Advancements, challenges, and future directions: a review, Energy Rep. 12 (Dec. 2024) 3566–3583, https://doi.org/10.1016/j.egyr.2024.09.038.
[104] R.J. Yang, Overcoming technical barriers and risks in the application of building integrated photovoltaics (BIPV): hardware and software strategies, Autom. Constr. 51 (Mar. 2015) 92–102, https://doi.org/10.1016/j.autcon.2014.12.005.
[105] C. Stanciu, D. Stanciu, Optimum tilt angle for flat plate collectors all over the World – a declination dependence formula and comparisons of three solar radiation models, Energy Convers. Manag. 81 (May 2014) 133–143, https://doi.org/10.1016/j.enconman.2014.02.016.
[106] M. A. Vaziri Rad, A. Toopshekan, P. Rahdan, A. Kasaeian, and O. Mahian, "A comprehensive study of techno-economic and environmental features of different solar tracking systems for residential photovoltaic installations," *Renew. Sustain. Energy Rev.*, vol. 129, p. 109923, Sep. 2020, doi: 10.1016/j.rser.2020.109923.